iScience

CellPress
OPEN ACCESS

Article

Neuronal loss of NCLX-dependent mitochondrial calcium efflux mediates age-associated cognitive decline

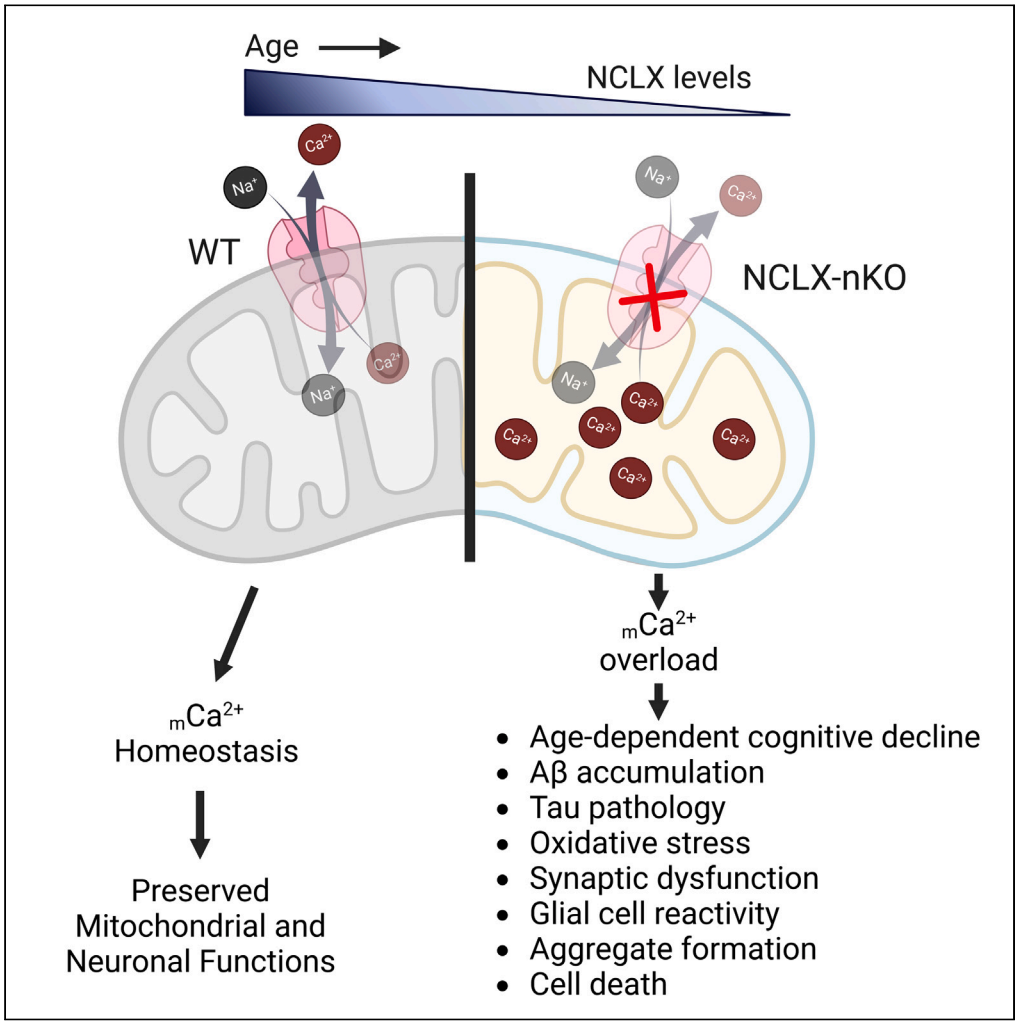

Pooja Jadiya, Henry M. Cohen, Devin W. Kolmetzky, Ashlesha A. Kadam, Dhanendra Tomar, John W. Elrod

elrod@temple.edu

Highlights

Reduced mitochondrial calcium efflux ($_{m}Ca^{2+}$) promotes age-associated cognitive decline

Deletion of neuronal NCLX is sufficient to promote Alzheimer's-like pathology

Neuronal mitochondrial dysfunction is sufficient to drive Aβ and tau pathology

Mitochondrial calcium exchange is a target for neurodegeneration, as occurs in AD

Jadiya et al., iScience *26*, 106296
March 17, 2023 © 2023 The Authors.
https://doi.org/10.1016/j.isci.2023.106296

iScience

CellPress
OPEN ACCESS

Article

Neuronal loss of NCLX-dependent mitochondrial calcium efflux mediates age-associated cognitive decline

Pooja Jadiya,[1,2] Henry M. Cohen,[1] Devin W. Kolmetzky,[1] Ashlesha A. Kadam,[2] Dhanendra Tomar,[1,2] and John W. Elrod[1,3,*]

SUMMARY

Mitochondrial calcium overload contributes to neurodegenerative disease development and progression. We recently reported that loss of the mitochondrial sodium/calcium exchanger (NCLX), the primary mechanism of $_{m}Ca^{2+}$ efflux, promotes $_{m}Ca^{2+}$ overload, metabolic derangement, redox stress, and cognitive decline in models of Alzheimer's disease (AD). However, whether disrupted $_{m}Ca^{2+}$ signaling contributes to neuronal pathology and cognitive decline independent of pre-existing amyloid or tau pathology remains unknown. Here, we generated mice with neuronal deletion of the mitochondrial sodium/calcium exchanger (NCLX, *Slc8b1* gene), and evaluated age-associated changes in cognitive function and neuropathology. Neuronal loss of NCLX resulted in an age-dependent decline in spatial and cued recall memory, moderate amyloid deposition, mild tau pathology, synaptic remodeling, and indications of cell death. These results demonstrate that loss of NCLX-dependent $_{m}Ca^{2+}$ efflux alone is sufficient to induce an Alzheimer's disease-like pathology and highlights the promise of therapies targeting $_{m}Ca^{2+}$ exchange.

INTRODUCTION

A decline in mitochondrial function is associated with normal aging and contributes to the development of various progressive neurodegenerative diseases. Decades ago, the mitochondrial theory of aging was proposed because of the significant role of mitochondria-derived reactive oxygen species (ROS) in aging.[1] Recent studies suggest that mitochondrial function directly impacts several essential aspects of aging and age-associated neurodegeneration, such as energetics, inflammation, cellular senescence, and redox stress.[2] Alzheimer's disease (AD) is the most common age-associated neurodegenerative disease and is characterized by memory loss, neuronal dysfunction, and the deposition of amyloid-beta (Aβ) and tau neurofibrillary tangles (NFTs) in the brain, specifically in the cortex and hippocampus. AD is classified as either familial or sporadic. Familial AD accounts for less than 5% of cases and is most often triggered by mutations in one of three genes, amyloid precursor protein (APP) and the presenilin encoding genes (PSEN1 and PSEN2). Sporadic AD has no known specific etiology and accounts for 90–95% of all AD diagnoses.[3] Discouragingly, following decades of research, this multifactorial disease remains incurable and the cellular and molecular mechanisms of AD pathogenesis remain poorly defined. The majority of AD phase II/III trials have targeted components of the amyloid-β cascade or tau pathway and have been largely unsuccessful.[4,5] Furthermore, many studies suggest that cognitive decline does not always correlate with Aβ and NFT deposition.[6–9] Taken together, these findings underscore the importance of defining alternative disease mechanisms driving the progression of AD.

Alterations in intracellular calcium ($_{i}Ca^{2+}$) homeostasis[10–13] and mitochondrial function[14,15] are critical to AD pathogenesis and occur before plaque deposition.[16–19] $_{i}Ca^{2+}$ signaling plays a crucial role in pre- and postsynaptic neurotransmission and membrane excitability. Impaired $_{i}Ca^{2+}$ signaling has been linked to AD pathogenesis via several different mechanisms including alterations in the inositol 1,4,5-trisphosphate receptor (IP_3R),[20–22] ryanodine receptor (RyR),[23,24] store-operated Ca^{2+} entry,[25,26] voltage-operated channels, and SERCA.[27] Furthermore, presenilin mutations and Aβ have been shown to increase the activity of RyR[28] and IP_3R,[29] suggesting exaggerated ER Ca^{2+} release in AD.[30] $_{i}Ca^{2+}$ enters the mitochondrial matrix via the mitochondrial calcium uniporter channel (mtCU).[31,32] $_{m}Ca^{2+}$ is a key regulator of various

[1]Cardiovascular Research Center, Department of Cardiovascular Sciences, Lewis Katz School of Medicine at Temple University, Philadelphia, PA 19140, USA

[2]Department of Internal Medicine, Wake Forest University School of Medicine, Winston-Salem, NC, 27157, USA

[3]Lead contact

*Correspondence: elrod@temple.edu

https://doi.org/10.1016/j.isci.2023.106296

This is an open access article under the CC BY-NC-ND license (http://creativecommons.org/licenses/by-nc-nd/4.0/).

mitochondrial processes and modulates the activity of multiple dehydrogenases (PDH, α-KGDH, and ICDH) in the Krebs cycle and ETC complexes to increase ATP production.[33,34] $_mCa^{2+}$ and the enzymatic activity of Ca^{2+}-dependent dehydrogenases are reported to be altered in neurodegenerative diseases, including AD,[15,18,35–38] highlighting the essential role of $_mCa^{2+}$ in the regulation of oxidative energy metabolism. In the brain, $_mCa^{2+}$ not only maintains energetics but also buffers $_iCa^{2+}$ and thus can regulate processes such as synaptic neurotransmission, synaptic vesicle exocytosis and cycling, neuronal excitability and axonal trafficking.[39,40] However, excessive uptake leads to $_mCa^{2+}$ overload and can cause rupture of the outer mitochondria membrane, opening of mitochondrial permeability transition pore (mPTP), loss of ATP production, excessive reactive oxygen species (ROS) generation, calpain activation and cell death.[41]

We recently reported that decreased expression of neuronal NCLX (the main mechanism for $_mCa^{2+}$ efflux[42]) causes $_mCa^{2+}$ overload in sporadic AD patients, 3xTg-AD mice, and *APP*swe cell lines.[18] Complete deletion of neuronal NCLX in the 3xTg-AD mouse model accelerated memory deficits and AD progression.[18] Furthermore, reducing $_mCa^{2+}$ overload by rescuing neuronal NCLX expression impedes AD-associated pathology and cognitive decline.[18] In support of this, multiple studies have reported $_mCa^{2+}$ overload as a feature of neurodegeneration. For example, Stavsky et al.[43] reported that a genetic loss of function of NCLX leads to $_mCa^{2+}$ overload and is linked with severe mental retardation. In addition, a recent study showed increased neuronal $_mCa^{2+}$ levels in the APP/PS1-Tg mouse model correlated with plaque deposition and neuronal demise.[35] Similarly, an increase in $_mCa^{2+}$ by overexpression of MCU in the cortex of mice resulted in neuronal dysfunction and gliosis.[36] In addition, increased ER-mitochondria interaction, which can augment $_mCa^{2+}$ overload, is reported in familial AD,[44] sporadic AD,[45] and in *sel-12* (*PSEN* ortholog) mutants in *C.elegans*.[46] In addition, loss of acute $_mCa^{2+}$ uptake via genetic ablation of *MCU* in cortical neurons is protective against ischemia-reperfusion injury without any metabolic abnormalities.[47] Altogether, these studies demonstrate that $_mCa^{2+}$ overload may be a central contributor to neuronal dysfunction.

In this study, we examined whether $_mCa^{2+}$ overload alone is sufficient to cause AD-like pathology. We tracked age-associated changes in memory and development of neuronal histopathology in mice with neuron-specific deletion of NCLX (*NCLX*-nKO) and controls. Loss of neuronal $_mCa^{2+}$ efflux caused a decline in cued recall and spatial working memory with a moderate increase in Aβ levels, tau phosphorylation, oxidative stress, and synaptic dysfunction. Our results demonstrate that loss of neuronal $_mCa^{2+}$ efflux and mitochondrial dysfunction promotes an AD-like phenotype, including age-associated cognitive decline.

RESULTS

Loss of NCLX-dependent neuronal $_mCa^{2+}$ efflux promotes cognitive decline

We have previously reported that loss of neuronal NCLX accelerates AD-pathology in the 3xTg-AD mouse model.[18] To examine NCLX expression during aging, we isolated protein from cortex of 2, 9, and 15-month-old control (Camk2a-cre) mice and noted an age-dependent reduction in NCLX expression (Figures S1A andS1B). To test whether impaired neuronal $_mCa^{2+}$ efflux alone is sufficient to elicit neuropathology we generated a neuron-restricted knockout of *Slc8b1*, the gene encoding the mitochondrial Na^+/Ca^{2+} exchanger, hereafter referred to as NCLX, by crossing *NCLX*$^{fl/fl}$ mice[48] with mice expressing a neuronal-restricted Cre recombinase (Camk2a-Cre) that primarily targets pyramidal neurons of the hippocampus, amygdala, and cerebral cortex[49] (Figure 1A). qPCR analysis of NCLX mRNA expression in the frontal cortex of 2-month-old *NCLX*$^{fl/fl}$ x Camk2a-Cre mice (NCLX-nKO) confirmed loss of NCLX compared to Camk2a-Cre controls (Figure 1B). Immunoblot analysis of NCLX in mitochondrial fractions purified from mouse brain identifies 50- and 65-kDa bands.[42] Western blot analysis confirmed loss of both the 50-kDa and 65-kDa forms of NCLX in the frontal cortex of 2-month-old mice without any significant alternation in the expression of components of the mitochondrial calcium uniporter channel (mtCU) (Figures 1C, 1D, and S1C–S1K).

Our recently published work showed that rescue of neuronal NCLX expression was sufficient to attenuate cognitive decline in 3xTg-AD mice.[18] To determine whether the loss of neuronal $_mCa^{2+}$ efflux alone is sufficient to promote age-associated cognitive decline we tested spatial working memory and cued/contextual recall in NCLX-nKO mice using a Y-maze spontaneous alternations test and fear-conditioning paradigm, respectively, at 6-, 9-, 12-, and 15-month of age. The Y-maze test revealed decreased spontaneous alternations in NCLX-nKO mice compared to controls at 15 months of age (Figure 1E), suggesting a decline in spatial working memory. No significant differences were observed in activity or motor function with the number of arm entries being similar between controls and NCLX-nKO mice (Figure 1F). Evaluation of associative memory by the fear-conditioning test revealed a decline in cued recall in 12- to 15-month-old

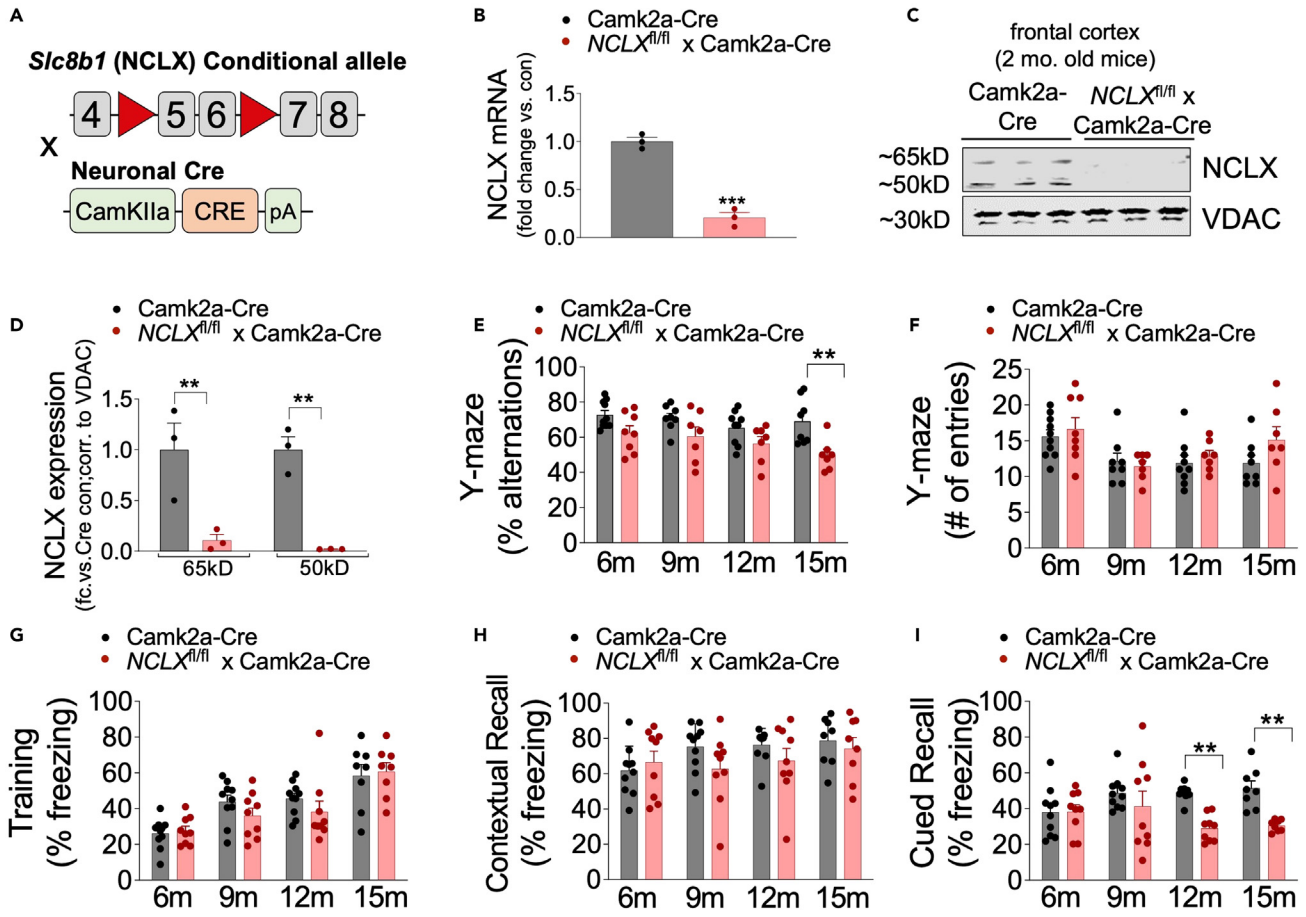

Figure 1. Loss of NCLX-dependent neuronal $_{m}Ca^{2+}$ efflux promotes cognitive decline

(A) Schematic of NCLX-nKO mice (*NCLX*$^{fl/fl}$ x Camk2a-Cre) mutant mouse strategy.

(B and C) (B) NCLX mRNA expression in tissue isolated from the frontal cortex of NCLX-nKO and age-matched controls (Camk2a-Cre). mRNA expression corrected to the housekeeping gene Rps13; expressed as fold change versus control, n = 3 for both groups. All data presented as mean ± SEM; ***p<0.001; two-tailed, unpaired t-test(C). Western blots for NCLX expression in tissue isolated from the cortex of 2-month-old *NCLX*$^{fl/fl}$ x Camk2a-Cre mice compared to age-matched control Camk2a-Cre mice. VDAC, voltage-dependent anion channel, served as mitochondrial loading controls.

(D) NCLX protein expression expressed as fold-change versus Camk2a-Cre con. corrected to a mitochondrial loading control VDAC in brain cortex of 2-month-old mice. All data presented as mean ± SEM; **p<0.01; two-way ANOVA with Sidak's multiple comparisons test.

(E and F) Y-maze spontaneous alternation test. (E) Percentage of spontaneous alternation. (F) Total number of arm entries.

(G–I) Fear-conditioning test. (G) Freezing responses in the training phase. (H) Contextual recall freezing responses, (I). Cued recall freezing responses. n = individual dots shown for each group in all graphs. All data presented as mean ± SEM. Data for percentage alternations, contextual and cued recall freezing response was analyzed using Prism (GraphPad) two-way ANOVA multiple comparison testing for an age effect with Dunnett's post-hoc test for comparison to age 6 months and comparison of genotype across all ages using a Bonferroni's multiple comparisons test, **p < 0.01. All comparisons were non-significant except those denoted. To ensure equivalent motor activity and behavior in the Y-maze and equivalent training for fear-conditioning behavioral testing data for Y-maze number of entries and freezing during training was analyzed using two-way ANOVA testing for comparison of genotype across all ages using a Bonferroni's multiple comparisons test. No statistical differences were noted.

NCLX-nKO mice compared to controls (Figure 1I). NCLX-nKO mice showed no impairments in contextual recall during training or recall phases (Figures 1G and 1H). We further validated motor function and coordination by challenging mice on a rotarod apparatus. 15-month-old NCLX-nKO mice showed no impairment and performed similarly to controls in the accelerating rotarod test (Figure S1L). These findings indicate a progressive age-associated decline in cognitive function in mice with loss of neuronal $_{m}Ca^{2+}$ efflux in the forebrain.

Loss of neuronal NCLX increases Aβ accumulation

Aβ accumulation in the brain is a central feature of AD pathogenesis. We have previously reported that loss of neuronal $_{m}Ca^{2+}$ efflux accelerates amyloidosis in 3xTg-AD mice.[18] Therefore, to determine whether

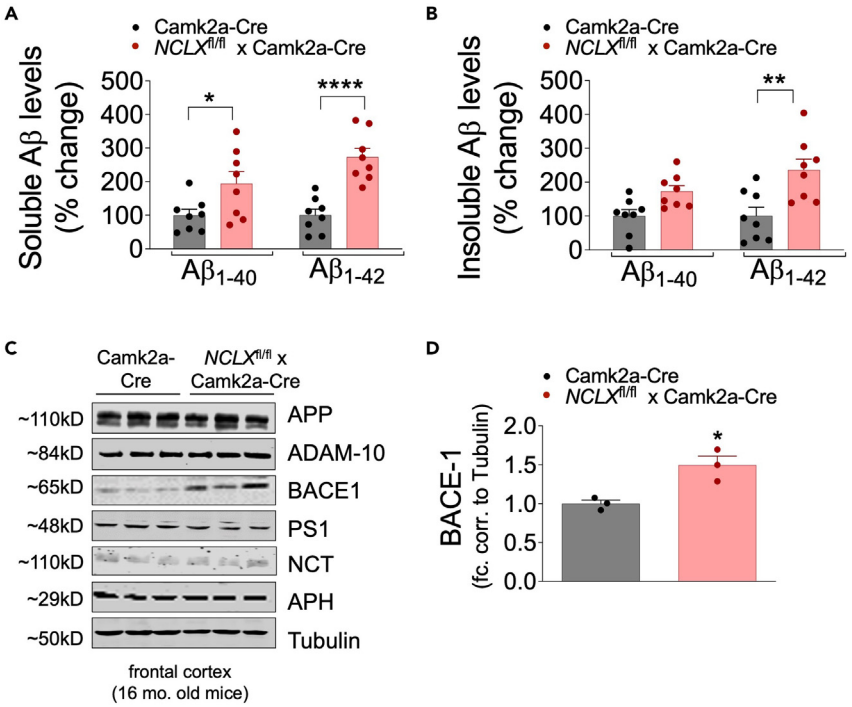

Figure 2. Loss of neuronal NCLX increases Aβ accumulation

(A and B) Soluble and insoluble $A\beta_{1-40}$ and $A\beta_{1-42}$ levels in the cortex of 16-month-old mice, measured by sandwich ELISA. n = individual dots are shown for each group in all graphs. All data presented as mean ± SEM; ****p<0.001, **p<0.01, *p<0.05; two-way ANOVA with Sidak's multiple comparisons test.

(C) Western blots for full-length APP, ADAM-10, BACE1, PS1, Nicastrin, APH, and tubulin (loading control) from cortex of 16-month-old NCLX-nKO and control mice, n = 3 for all groups.

(D) BACE-1 protein expression expressed as fold change versus Camk2a-Cre con. corrected to tubulin loading control from frontal cortex of 2-month-old mice. All data presented as mean ± SEM; *p<0.05; two-tailed, unpaired t-test.

genetic ablation of neuronal NCLX impacts Aβ metabolism or amyloidosis, we performed an Aβ ELISA and immunohistochemistry assays. NCLX-nKO and controls were euthanized at 16 months of age and brain cortex homogenates were assayed for total $A\beta_{1-40}$ and $A\beta_{1-42}$ peptide levels in the RIPA-soluble and insoluble fractions. NCLX-nKO cortical samples were found to have significantly increased total $A\beta_{1-40}$ and $A\beta_{1-42}$ in soluble fraction as compared to controls (Figures 2A and 2B). These results suggest that the loss of NCLX increases the levels of the amyloidogenic peptide. Next, we examined the protein levels of Aβ precursor protein (APP) and proteases involved in its metabolism. NCLX-nKO cortical samples showed a significant increase in the expression of β-secretase (BACE-1) (Figures 2C and 2D), as compared to controls at 16 months. No differences in the expression of total APP or γ-secretase complex associated proteins (PS1, NCT, and APH1 subunit) were observed between groups (Figures 2C and S2A–S2E).

Neuronal loss of NCLX increases tau pathology

Hyperphosphorylation of microtubule-associated protein (tau) and the formation of neurofibrillary tangles (NFTs) are prominent characteristics of various neurodegenerative diseases, such as frontotemporal dementia, chronic traumatic encephalopathy, and AD. To determine if loss of neuronal $_mCa^{2+}$ efflux impacts tau pathology we performed Western blots to examine the total expression and phosphorylation of tau at various residues, including S202/T205, T231/S235, and T181 and S396 as recognized by the antibodies AT8, AT180, AT270, and PHF-13, respectively. We observed an increase in phosphorylation at T231/S235 (AT180 immunoreactivity) and at S202/T205 (AT8 immunoreactivity) in cortical lysates from NCLX-nKO mice with no significant change in total tau or phosphorylation of other residues (Figures 3A–3E). These results were corroborated by our immunohistochemistry results showing increased T231/S235 tau phosphorylation (Figures 3F–3H) in the CA1 pyramidal region of the hippocampus. These results suggest genetic ablation of neuronal $_mCa^{2+}$ efflux is sufficient to increase tau pathology with aging.

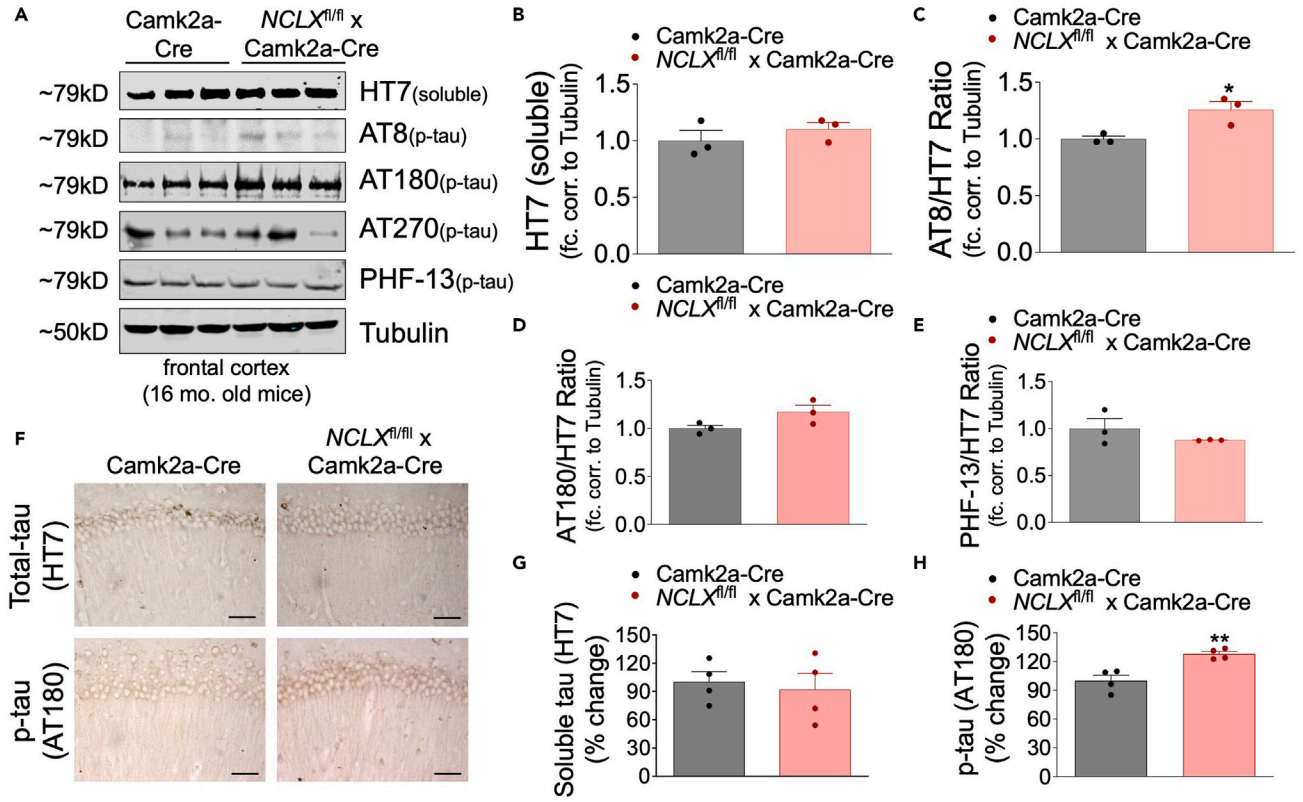

Figure 3. Loss of NCLX increases tau-pathology

(A) Representative western blots of soluble total tau (HT7), and phosphorylated tau at residues S202/T205 (AT8), T231/S235 (AT180), T181 (AT270), and S396 (PHF13) in cortex homogenates of 16-month-old mice, n = 3 for all groups.

(B–E) Densitometric analysis of western blots shown in Figure 3A expressed as fold-change versus Camk2a-Cre con. Corrected to a loading control tubulin.

(F) Representative immunohistochemical staining for total tau (HT7) and phospho-tau T231/S235 (AT180) in hippocampus of NCLX-nKO and control mice; scale bar = 50 μM.

(G and H) Quantification of the integrated optical density area of HT7 and AT180 immunoreactivity, n = 4 for all groups. All data presented as mean ± SEM; **p<0.01, *p<0.05; two-tailed, unpaired t-test.

Neuronal loss of $_{m}Ca^{2+}$ efflux leads to redox imbalance, decreased synaptic stability and neuronal loss

Increased lipid peroxidation is indicative of oxidative stress that occurs early in neurodegenerative diseases, such as AD.[50,51] To determine the effect of neuronal loss of $_{m}Ca^{2+}$ efflux on redox status, we examined lipid peroxidation by 4-hydroxy-2-nonenal (4-HNE) staining in 16-month-old NCLX-nKO brains and controls. NCLX-nKO mice displayed a ~35% increase in 4-HNE staining in the cortex, as compared to controls (Figures 4A and 4B).

AD is characterized by loss of synaptic function.[52–54] Loss of NCLX in primary hippocampal neurons is reported to cause massive synaptic impairment and deficits in long-term potentiation.[43] Considering the important role of NCLX in regulating neuronal transmission, we next examined how loss of neuronal NCLX affects synaptic integrity and stability. Postsynaptic density protein 95 (PSD-95) is a major synaptic scaffold protein regulating glutamate receptor trafficking and localization and plays an important role in synaptic plasticity, development, and learning.[55,56] Synaptophysin (SYP) is a highly abundant presynaptic vesicular membrane glycoprotein implicated in biogenesis and endocytosis of synaptic vesicles, synapse formation, and regulation of synaptic transmission.[57,58] Loss of either PSD-95 or SYP is indicative of synaptic instability and is an early marker of neurodegeneration.[59,60] Western blot analysis revealed significant decreases in both SYP and PSD-95 expression in the frontal cortex of NCLX-nKO mice (Figures 4C–4E). These findings suggest that loss of neuronal $_{m}Ca^{2+}$ efflux alone promotes synaptic dysfunction.

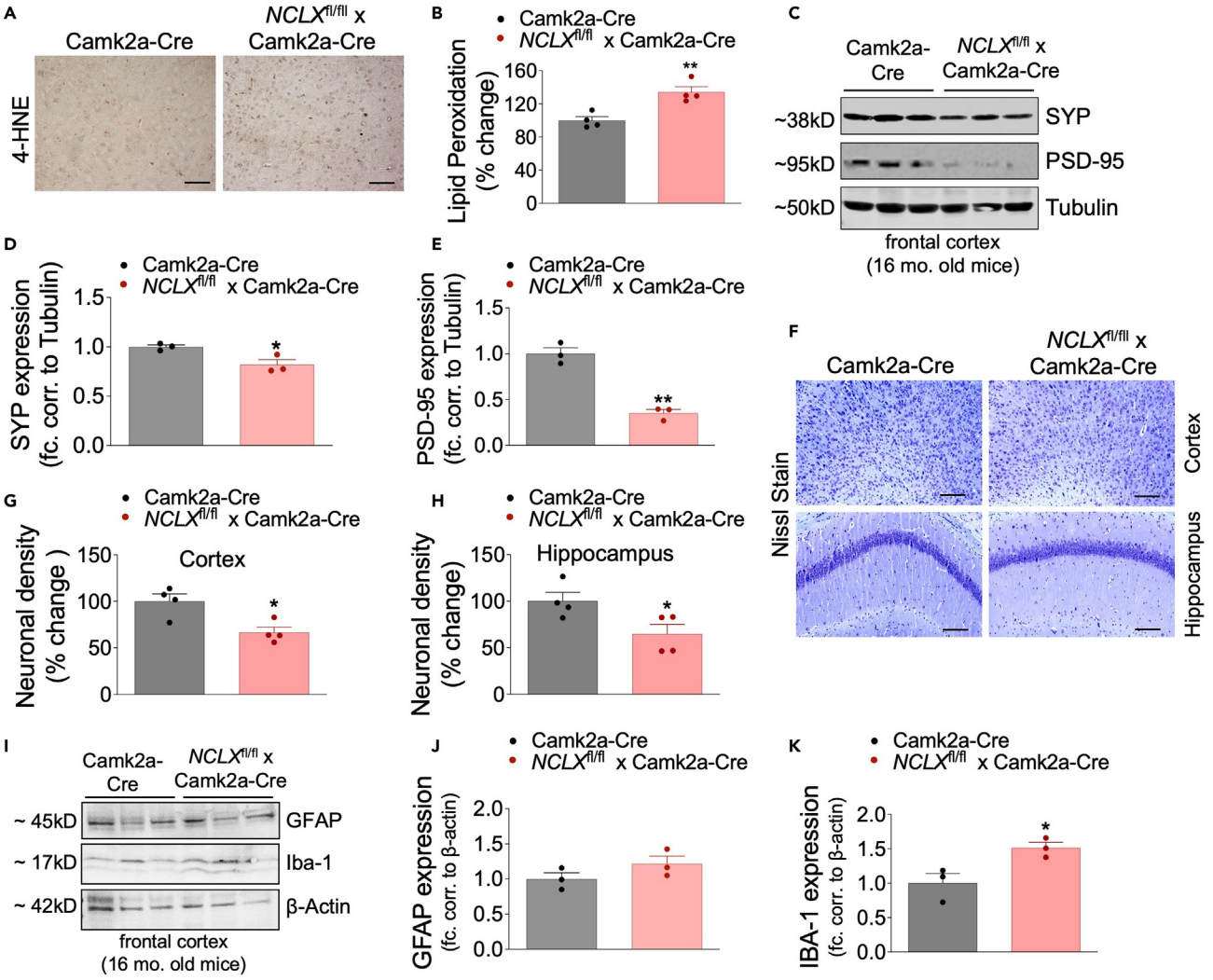

Figure 4. Neuronal loss of $_{m}Ca^{2+}$ efflux leads to redox imbalance, decreased synaptic stability and neuronal loss

(A) Representative images of 4-HNE immunohistochemical staining in cortex and hippocampus of 16-month-old NCLX-nKO and control mice.

(B) Percent change in 4-HNE-integrated optical density area corrected to Camk2a-Cre controls. N = 4 for all groups, scale bar = 50 μM.

(C) Western blots for SYP and PSD-95 expression in tissue isolated from the cortex of 16-month-old-mice, n = 3 for all groups.

(D and E) Densitometric analysis of western blots shown in Figure 4C, expressed as fold change versus Camk2a-Cre con. corrected to loading control tubulin.

(F) Representative image of Nissl staining in cortex and hippocampus of 16-month-old mice to detect neuronal density.

(G and H) Quantitative analysis of Nissl positive cells in cortex and hippocampus areas of brain sections expressed as percent change versus Camk2a-Cre controls. n = 4 for all groups, scale bar = 50 μM.

(I) Western blots for GFAP and IBA1 expression in cortex of 16-month-old-mice, n = 3 for all groups.

(J and K) Densitometric analysis of western blots shown in Figure 4I, expressed as fold change versus Camk2a-Cre con. corrected to loading control β-actin.

All data presented as mean ± SEM; **p<0.01, *p<0.05; two-tailed, unpaired t-test.

Next, we examined if NCLX-nKO mice experience neuronal loss, we performed Nissl staining using cresyl violet acetate. The neuronal density was measured in 16-month-old NCLX-nKO and controls brain section. NCLX-nKO mice exhibited significantly reduced Nissl-positive staining in the cortex and hippocampus relative to controls. (Figures 4F–4H). Increased glial cell reactivity is usually associated with the death of neurons and the activation of astrocytes and microglia is a critical pro-inflammatory mechanisms in AD[59,60] that can be evaluated by the expression of biomarkers. We analyzed protein levels of the glial fibrillary acidic protein (GFAP), a marker of astrocyte reactivity,[61] and Ionized calcium-binding adaptor molecule 1 (Iba1), a marker for microglia activation. The expression of Iba1 was increased in brain homogenates isolated from NCLX-nKO mice compared to controls, without significant changes in GFAP expression (Figures 4I–4K), suggesting that loss of neuronal NCLX may elicit glial activation.

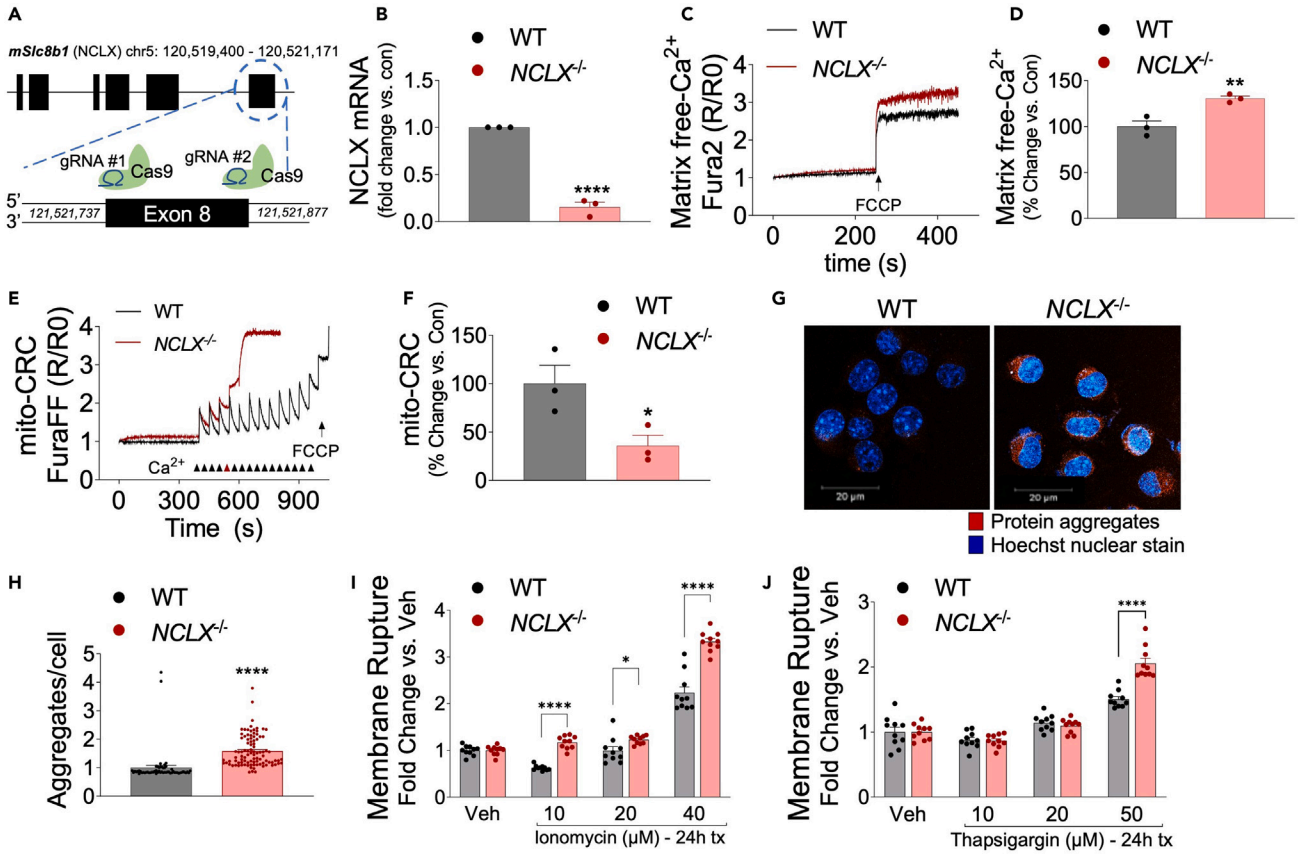

Figure 5. Loss of NCLX increases $_{m}Ca^{2+}$ overload, aggregate formation, and cell death

(A) Schematic for generation of NCLX knockout cell line ($NCLX^{-/-}$) using CRISPR/SpCas9.

(B) NCLX mRNA expression in $NCLX^{-/-}$ and controls (WT) N2a cells, corrected to the housekeeping gene, Rps13; expressed as fold change versus control, n = 3 for both groups. All data presented as mean ± SEM; ****p<0.001; two-tailed, unpaired t-test.

(C) Representative traces for basal $_{m}Ca^{2+}$ content.

(D and E) (D) Quantification of $_{m}Ca^{2+}$ content, n = 3 for both groups. All data presented as mean ± SEM; **p<0.001; two-tailed, unpaired t-test(E). Representative recordings of $_{m}Ca^{2+}$ retention capacity.

(F and G) (F)Percent change in $_{m}Ca^{2+}$ retention capacity versus N2a control cells, n = 3 for both groups. All data presented as mean ± SEM; *p<0.05; two-tailed, unpaired t-test(G). Representative images of intracellular protein aggregates in $NCLX^{-/-}$ and WT cells stained with Proteostat aggresome detection reagent (red) and Hoechst 33,342 nuclear stain (blue), scale bars = 20-µm.

(H) Total aggregates per cell, n = 96 for $NCLX^{-/-}$ and n = 58 for WT N2a control. All data presented as mean ± SEM; ****p<0.001; two-tailed, unpaired t-test.

(I and J) $NCLX^{-/-}$ and WT cells were assessed for plasma membrane rupture, Sytox Green, after treatment with (I). Ionomycin (10–40 µM), (J). thapsigargin (10–50 µM), n = 10 for both groups. All data presented as mean ± SEM; ***p<0.001, **p<0.01, *p<0.05; two-way ANOVA with Sidak's multiple comparisons test.

Loss of NCLX increases $_{m}Ca^{2+}$ overload, aggregate formation, and cell death

To evaluate how the loss of NCLX contributes to AD progression and mitochondrial dysfunction, we generated stable NCLX knockout (*Slc8b1* deletion; $NCLX^{-/-}$) neuroblastoma (N2a) cell lines using CRISPR/SpCas9. SpCas9 was targeted to exon 8 of *Slc8b1* by using a double guide RNA strategy (Figure 5A). After hygromycin selection, clonal $NCLX^{-/-}$ cell lines were examined for loss of mRNA by qPCR. $NCLX^{-/-}$ cell lines showed a significant loss of NCLX expression compared to wild-type (WT) N2a controls (Figure 5B). Next, matrix Ca^{2+} levels in $NCLX^{-/-}$ and WT cells were measured in a permeabilized cell system using the ratiometric reporter Fura2 (Figures 5C and 5D). Equal numbers of cells from both groups were treated with digitonin and thapsigargin and the protonophore, FCCP was added after reaching a steady state recording, to collapse $\Delta\Psi$ and initiate the release of all matrix-free Ca^{2+} (Figure 5C). Consistent with previous study,[43] quantification of $_{m}Ca^{2+}$ content showed that loss of NCLX causes a significant increase in $_{m}Ca^{2+}$ content compared to WT (Figure 5D). Next, we employed a $_{m}Ca^{2+}$ retention capacity assay (mitoCRC) using the ratiometric reporters FuraFF (Ca^{2+}) and added repetitive boluses of 10-µM Ca^{2+} until the collapse of $\Delta\Psi$. $NCLX^{-/-}$ cells showed decreased mitoCRC by ~65% compared to WT cells, suggesting

increased susceptibility to Ca^{2+}-dependent permeability transition pore opening (Figures 5E and 5F). Overall, these data suggest that loss of NCLX causes $_mCa^{2+}$ overload and decreases CRC.

Protein misfolding and aggregation is a hallmark feature of neurodegenerative diseases including Alzheimer's disease, Parkinson's disease, Huntington's disease, dementia with Lewy bodies, and Amyotrophic Lateral Sclerosis, among others. To test if loss of NCLX impacts protein aggregation, we performed a ProteoStat Aggresome detection assay. *NCLX*$^{-/-}$ cells exhibited a significantly increased abundance (~50% increase) of intracellular 'amyloid-like' aggregates compared to WT (Figures 5G and 5H). These results suggest that loss of NCLX alone can drive protein aggregation.

$_mCa^{2+}$ overload is strongly associated with cell death. To further evaluate how loss of NCLX modulates cell death, cells from both groups were treated with varying concentrations of necrotic agonists ionomycin (general intracellular calcium stress,10–40 μM) and thapsigargin (ER Ca^{2+} stress, 10–50 μM) and examined plasma membrane rupture, a hallmark of cell death using Sytox Green. *NCLX*$^{-/-}$ cells demonstrated significantly increased plasma membrane rupture compared to WT at most doses (Figures 5I and 5J). Altogether, these results suggest that the inhibition of $_mCa^{2+}$ efflux causes $_mCa^{2+}$ overload, amyloid-like protein aggregation, and potentiates cell death.

DISCUSSION

In this study, we utilized a genetic loss-of-function model to show that impaired mitochondrial calcium efflux is sufficient to promote an AD-like phenotype. We have previously reported that diminished $_mCa^{2+}$ efflux contributes to $_mCa^{2+}$ overload and accelerates pathogenesis of AD, including cognitive decline, in Aβ and tau genetic models. In addition, we previously reported that rescue of neuronal NCLX expression was sufficient to attenuate cognitive deficits and neuropathology in 3xTg-AD mouse model.[18] It is important to note that 3xTg-AD mutant mice harbor three gene mutations associated with familial AD: Presenilin 1 (Psen1, M146V homozygous knock-in), amyloid beta precursor protein (APPswe, KM670/671NL transgene) and microtubule-associated protein tau (MAPT, P301L transgene) and that these mice demonstrate progressive $_mCa^{2+}$ overload with aging. Thus, cognitive decline is more rapid and profound in the 3xTg-AD mice after neuronal deletion of NCLX compared to NCLX-nKO as it is exacerbating pre-existing $_mCa^{2+}$ overload, a pathologic feature of disease. Intriguingly, here we found that loss of neuronal NCLX expression causes AD-like dysfunction, including memory loss, Aβ plaque burden, tau hyperphosphorylation, oxidative stress, and loss of synaptic integrity in aged mice (12–16 months old) in the absence of any AD or neurodegenerative genetic predisposition (i.e., no expression of familial AD mutant genes). Our study demonstrates that loss of neuronal NCLX and resulting $_mCa^{2+}$ overload causes neurodegenerative pathology and age associated cognitive decline.

Our hypothesis, that $_mCa^{2+}$ overload is a driver of AD-pathology, is supported by several studies. Recently, *NCLX*-knockout primary hippocampal neurons showed $_mCa^{2+}$ overload, depolarization of mitochondrial membrane potential and reduced calcium clearance during neuronal activity.[43] Even more striking the same group showed that an NCLX loss-of-function mutation is linked with severe mental retardation and that loss of NCLX causes synaptic impairment and long-term plasticity deficits.[43] These data strongly support our findings that NCLX-nKO mice experience an age-dependent decline in spatial memory and cued recall, moderate amyloid deposition, mild tau hyperphosphorylation, and synaptic remodeling. $_mCa^{2+}$ overload is a trigger for mPTP opening that leads to cell death.[62–65] Inhibition of mPTP has shown beneficial effects against neuronal cell death resulting from glutamate excitotoxicity,[66] traumatic brain injury,[67] ischemia-reperfusion injury,[68] Parkinson's disease,[69] and AD.[62,70] The loss of either MCUB (a negative regulator of the mtCU)[71] or MICU1 (gatekeeper of the mtCU at low cytosolic Ca^{2+} levels)[72,73] promotes $_mCa^{2+}$ overload. Important to the current study, reduced expression of mtCU-associated proteins, including MICU1 and MCUB, is reported in the frontal cortex of sporadic AD patients and 3xTg-AD mice.[18] In addition, loss of MICU1 (homozygous deletion of exon 1) results in sporadic neurological and muscular defects in humans, which is characterized by the $_mCa^{2+}$ overload, diminished metabolism, early muscle weakness, myofiber damage, impaired cognition, and an extrapyramidal movement disorder.[74–76] Furthermore, MICU1 variants are implicated in congenital brain malformation, characterized by white matter abnormalities, cerebellar dysplasia, and acute encephalopathy.[77] Recently, a parallel line of research has found myopathy with extrapyramidal symptoms in patients carrying nonsense mutations in the *MICU1* gene (c.385C>T; p.(R129*)),[78] (c.52C>T; p.(Arg18*) and c.553C>T; p.(Arg185*)).[79] Consistent with human studies, deletion of *Micu1* in mice causes marked ataxia and muscular defects.[80,81] Recently, our group reported

that reducing $_{m}Ca^{2+}$ influx by neuronal-specific deletion of *MCU* in the 3xTg-AD mouse model reduces AD progression.[82] In summary, a growing body of evidence implicates $_{m}Ca^{2+}$ exchange dysregulation in a plethora of neurodegenerative diseases.

However, numerous fundamental questions remain unanswered. For example, why are neurons in aged mice susceptible to $_{m}Ca^{2+}$ overload and how is the loss of NCLX or remodeling of the mtCU coincide with the development of AD? What are the molecular mechanisms underlying the proteomic remodeling of $_{m}Ca^{2}$ machinery? Furthermore, it remains enigmatic whether $_{m}Ca^{2+}$ dysregulation is specific to AD or central to other neurodegenerative diseases. We hypothesize that increased $_{m}Ca^{2+}$ content is a mechanism for 'stressed' neurons to meet their energetic demands, enhancing mitochondrial metabolism by augmenting dehydrogenase activity (PDH and αKGD), Krebs cycle flux, and ATP production.[33,83] This early adaptive response ultimately becomes maladaptive through sustained stress, leading to $_{m}Ca^{2+}$ overload and mitochondrial dysfunction. Previous research suggests that the calcium buffering capacity of mitochondria declines with aging, making mitochondria more prone to $_{m}Ca^{2+}$ overload.[84] These observations further support our hypothesis of $_{m}Ca^{2+}$ mishandling during aging that ultimately can contribute to the development of neurodegenerative diseases.

It's clear that $_{m}Ca^{2+}$ overload is a primary upstream mechanism in AD-like pathology; yet it remains unknown how loss of NCLX results in Aβ and tau aggregation. There are likely many key contributors such as oxidative stress, metabolic dysfunction, and cell death that get activated in response to $_{m}Ca^{2+}$ dysregulation, causing AD progression. It's also possible that there is a feedback loop between $_{m}Ca^{2+}$ dysregulation and AD-pathology. For example, it is reported that increased $_{m}Ca^{2+}$ uptake and glutamate excitotoxicity lead to oxidative stress in a number of studies.[72,85,86] This paradigm further corroborates our finding of increased lipid peroxidation following loss of neuronal NCLX. Intracellular Ca^{2+} signaling is reported to modulate BACE1 expression and turnover. Furthermore, reports suggest that oxidative stress increases BACE1 expression, Aβ accumulation, tau hyperphosphorylation, and synaptic dysfunction.[87,88] Given the noted relationship between $_{m}Ca^{2+}$ overload and ROS, its plausible that a maladaptive pathway may contribute to Aβ processing. Also, oxidative stress has been shown to impair respiration by reducing glucose uptake and limiting substrate availability.[89] In addition, $_{i}Ca^{2+}$ signaling is also believed to enhance reactive nitrogen species (RNS),[90] which can impair mitochondrial metabolism through inhibitory S-nitrosylation of Krebs cycle enzymes such as aconitase, isocitrate dehydrogenase, alpha-ketoglutarate dehydrogenase[91,92] and electron transport chain (ETC) complexes.[93,94] The resulting dysfunctional mitochondrial metabolism can further disrupt axonal transport of mitochondria and other APP-associated proteins, including BACE-1.[95,96] Of interest, impaired axonal transport is an early contributor of AD[95,96] that has diverse effects including compromised mitochondrial quality control mechanisms, leading to protein aggregation, neuronal dysfunction, and cell death.[97] We hypothesize that impaired mitochondrial quality control and protein aggregation can potentiate mitochondrial dysfunction such as oxidative stress and cell death, creating a vicious cycle underlying the progression of AD. In addition, the mechanism of synaptic dysfunction and gliosis in a $_{m}Ca^{2+}$ overloaded state might be associated with Aβ deposition. It is known that Aβ impacts glial activation that can subsequently drive synapse dysfunction and neuronal death, and that vice versa glial cell activation can modulate Aβ production through several mechanisms. These mechanisms need to be explored in the future and might include changes in neuronal ionic homeostasis and an alternation of various transporters, exchangers (present on the plasma membrane, and ER), and Ca^{2+}-handling proteins that are responsible for various neuronal functions.[98,99] In conclusion, $_{m}Ca^{2+}$ dysregulation is sufficient to perturb neuronal mitochondrial function and drive age-associated neurodegeneration and cognitive decline. This study, coupled with the reports mentioned above, advocates for correcting $_{m}Ca^{2+}$ dysregulation by restoring NCLX-dependent $_{m}Ca^{2+}$ efflux capacity as a promising therapeutic strategy in treating neurodegenerative diseases. The phosphorylation of *NCLX* by PKA, which potentiates *NCLX* mediated $_{m}Ca^{2+}$ efflux, is effective in preventing dopamine-dependent demise of PINK1 deficient neurons,[100] a cellular Parkinson's model. In combination with past work demonstrating that genetic rescue of NCLX slows cognitive decline in mouse models of AD, these findings further support that modulation of $_{m}Ca^{2+}$ handling, specifically via activation of *NCLX,* could be an effective strategy to treat neurodegenerative diseases.

Limitations of the study

This report suggests that impaired $_{m}Ca^{2+}$ efflux is sufficient to drive Alzheimer's disease-like, age-associated dementia. One limitation is that the current results did not identify the downstream molecular

mechanisms by which loss of $_mCa^{2+}$ efflux results in neuropathology. Another caveat of this study is the utilization of mouse models that fail to recapitulate all the features of cognitive decline in humans. In general the field is hampered by a lack of animal models that faithfully capture non-familial or sporadic AD. Such models are needed to test if augmenting $_mCa^{2+}$ efflux is indeed a viable therapeutic strategy.

STAR★METHODS

Detailed methods are provided in the online version of this paper and include the following:

- KEY RESOURCES TABLE
- RESOURCE AVAILABILITY
  - Lead contact
  - Materials availability
  - Data and code availability
- EXPERIMENTAL MODEL AND SUBJECTDETAILS
  - Neuronal-specific NCLX knockout (*NCLX*$^{fl/fl}$ x Camk2a-Cre) mouse
- METHOD DETAILS
  - Immunohistochemistry
  - Biochemical and western blot analysis
  - Memory tests
  - Y-maze of spontaneous alternation
  - Contextual and cued fear conditioning
  - Rotarod test
  - Assessment of lipid peroxidation
  - Nissl staining
  - Cell culture and generation of NCLX knockout cells
  - qPCR mRNA analysis
  - Quantification of $_mCa^{2+}$ content and retention capacity
  - Membrane rupture assay
  - Detection of protein aggregation
- QUANTIFICATION AND STATISTICAL ANALYSIS

SUPPLEMENTAL INFORMATION

Supplemental information can be found online at https://doi.org/10.1016/j.isci.2023.106296.

ACKNOWLEDGMENTS

We thank Trevor Tierney and Alycia Hildebrand for technical assistance in the Elrod Lab. The graphical abstract was created with BioRender.com. Support for this work was provided by grants from the NIH: R01NS121379, R01HL136954, R01HL142271, 3R01HL123966-05S1, P01HL147841, P01HL134608; AHA: 20EIA35320226, and Pennsylvania Department of Health CURE Award (420792) to J.W.E.; NIH R00AG065445, P30 AG072947 to P.J., and NIH R00DK120876 to D.T.

AUTHOR CONTRIBUTIONS

J.W.E. conceived the project; J.W.E. and P.J. contributed to study design, data analysis, and writing the paper; P.J., H.C., A.K., D.T., and D.K. performed experiments, data collection, and interpretation, J.W.E., P.J., H.C., and D.T. edited the manuscript and provided expertise with data interpretation.

DECLARATION OF INTERESTS

The authors declare no competing financial interests related to this work. J.W.E. is a paid consultant for Mitobridge, Inc., An Astellas Company.

Received: October 11, 2021
Revised: December 12, 2022
Accepted: February 20, 2023
Published: February 28, 2023

REFERENCES

1. Harman, D. (1972). The biologic clock: the mitochondria? J. Am. Geriatr. Soc. *20*, 145–147. https://doi.org/10.1111/j.1532-5415.1972.tb00787.x.

2. Sun, N., Youle, R.J., and Finkel, T. (2016). The mitochondrial basis of aging. Mol. Cell *61*, 654–666. https://doi.org/10.1016/j.molcel.2016.01.028.

3. Jack, C.R., Jr., Bennett, D.A., Blennow, K., Carrillo, M.C., Dunn, B., Haeberlein, S.B., Holtzman, D.M., Jagust, W., Jessen, F., Karlawish, J., et al. (2018). NIA-AA Research Framework: toward a biological definition of Alzheimer's disease. Alzheimers Dement. *14*, 535–562. https://doi.org/10.1016/j.jalz.2018.02.018.

4. Mehta, D., Jackson, R., Paul, G., Shi, J., and Sabbagh, M. (2017). Why do trials for Alzheimer's disease drugs keep failing? A discontinued drug perspective for 2010-2015. Expert Opin. Investig. Drugs *26*, 735–739. https://doi.org/10.1080/13543784.2017.1323868.

5. Panza, F., Lozupone, M., Watling, M., and Imbimbo, B.P. (2019). Do BACE inhibitor failures in Alzheimer patients challenge the amyloid hypothesis of the disease? Expert Rev. Neurother. *19*, 599–602. https://doi.org/10.1080/14737175.2019.1621751.

6. Giannakopoulos, P., Herrmann, F.R., Bussière, T., Bouras, C., Kövari, E., Perl, D.P., Morrison, J.H., Gold, G., and Hof, P.R. (2003). Tangle and neuron numbers, but not amyloid load, predict cognitive status in Alzheimer's disease. Neurology *60*, 1495–1500. https://doi.org/10.1212/01.wnl.0000063311.58879.01.

7. Guillozet, A.L., Weintraub, S., Mash, D.C., and Mesulam, M.M. (2003). Neurofibrillary tangles, amyloid, and memory in aging and mild cognitive impairment. Arch. Neurol. *60*, 729–736. https://doi.org/10.1001/archneur.60.5.729.

8. Mostafavi, S., Gaiteri, C., Sullivan, S.E., White, C.C., Tasaki, S., Xu, J., Taga, M., Klein, H.U., Patrick, E., Komashko, V., et al. (2018). A molecular network of the aging human brain provides insights into the pathology and cognitive decline of Alzheimer's disease. Nat. Neurosci. *21*, 811–819. https://doi.org/10.1038/s41593-018-0154-9.

9. Neff, R.A., Wang, M., Vatansever, S., Guo, L., Ming, C., Wang, Q., Wang, E., Horgusluoglu-Moloch, E., Song, W.M., Li, A., et al. (2021). Molecular subtyping of Alzheimer's disease using RNA sequencing data reveals novel mechanisms and targets. Sci. Adv. *7*, eabb5398. https://doi.org/10.1126/sciadv.abb5398.

10. Alzheimer's Association Calcium Hypothesis Workgroup (2017). Calcium Hypothesis of Alzheimer's disease and brain aging: a framework for integrating new evidence into a comprehensive theory of pathogenesis. Alzheimers Dement. *13*, 178–182.e17. https://doi.org/10.1016/j.jalz.2016.12.006.

11. Bezprozvanny, I., and Mattson, M.P. (2008). Neuronal calcium mishandling and the pathogenesis of Alzheimer's disease. Trends Neurosci. *31*, 454–463. https://doi.org/10.1016/j.tins.2008.06.005.

12. Briggs, C.A., Chakroborty, S., and Stutzmann, G.E. (2017). Emerging pathways driving early synaptic pathology in Alzheimer's disease. Biochem. Biophys. Res. Commun. *483*, 988–997. https://doi.org/10.1016/j.bbrc.2016.09.088.

13. Khachaturian, Z.S. (1989). Calcium, membranes, aging, and Alzheimer's disease. Introduction and overview. Ann. N. Y. Acad. Sci. *568*, 1–4. https://doi.org/10.1111/j.1749-6632.1989.tb12485.x.

14. Swerdlow, R.H. (2020). The mitochondrial hypothesis: dysfunction, bioenergetic defects, and the metabolic link to Alzheimer's disease. Int. Rev. Neurobiol. *154*, 207–233. https://doi.org/10.1016/bs.irn.2020.01.008.

15. Jadiya, P., Garbincius, J.F., and Elrod, J.W. (2021). Reappraisal of metabolic dysfunction in neurodegeneration: focus on mitochondrial function and calcium signaling. Acta Neuropathol. Commun. *9*, 124. https://doi.org/10.1186/s40478-021-01224-4.

16. Teo, E., Ravi, S., Barardo, D., Kim, H.S., Fong, S., Cazenave-Gassiot, A., Tan, T.Y., Ching, J., Kovalik, J.P., Wenk, M.R., et al. (2019). Metabolic stress is a primary pathogenic event in transgenic Caenorhabditis elegans expressing pan-neuronal human amyloid beta. Elife *8*, e50069. https://doi.org/10.7554/eLife.50069.

17. Chou, J.L., Shenoy, D.V., Thomas, N., Choudhary, P.K., Laferla, F.M., Goodman, S.R., and Breen, G.A.M. (2011). Early dysregulation of the mitochondrial proteome in a mouse model of Alzheimer's disease. J. Proteomics *74*, 466–479. https://doi.org/10.1016/j.jprot.2010.12.012.

18. Jadiya, P., Kolmetzky, D.W., Tomar, D., Di Meco, A., Lombardi, A.A., Lambert, J.P., Luongo, T.S., Ludtmann, M.H., Praticò, D., and Elrod, J.W. (2019). Impaired mitochondrial calcium efflux contributes to disease progression in models of Alzheimer's disease. Nat. Commun. *10*, 3885. https://doi.org/10.1038/s41467-019-11813-6.

19. Völgyi, K., Badics, K., Sialana, F.J., Gulyássy, P., Udvari, E.B., Kis, V., Drahos, L., Lubec, G., Kékesi, K.A., and Juhász, G. (2018). Early presymptomatic changes in the proteome of mitochondria-associated membrane in the APP/PS1 mouse model of Alzheimer's disease. Mol. Neurobiol. *55*, 7839–7857. https://doi.org/10.1007/s12035-018-0955-6.

20. Cai, C., Lin, P., Cheung, K.H., Li, N., Levchook, C., Pan, Z., Ferrante, C., Boulianne, G.L., Foskett, J.K., Danielpour, D., and Ma, J. (2006). The presenilin-2 loop peptide perturbs intracellular Ca2+ homeostasis and accelerates apoptosis. J. Biol. Chem. *281*, 16649–16655. https://doi.org/10.1074/jbc.M512026200.

21. Cheung, K.H., Mei, L., Mak, D.O.D., Hayashi, I., Iwatsubo, T., Kang, D.E., and Foskett, J.K. (2010). Gain-of-function enhancement of IP3 receptor modal gating by familial Alzheimer's disease-linked presenilin mutants in human cells and mouse neurons. Sci. Signal. *3*, ra22. https://doi.org/10.1126/scisignal.2000818.

22. Cheung, K.H., Shineman, D., Müller, M., Cárdenas, C., Mei, L., Yang, J., Tomita, T., Iwatsubo, T., Lee, V.M.Y., and Foskett, J.K. (2008). Mechanism of Ca2+ disruption in Alzheimer's disease by presenilin regulation of InsP3 receptor channel gating. Neuron *58*, 871–883. https://doi.org/10.1016/j.neuron.2008.04.015.

23. Rybalchenko, V., Hwang, S.Y., Rybalchenko, N., and Koulen, P. (2008). The cytosolic N-terminus of presenilin-1 potentiates mouse ryanodine receptor single channel activity. Int. J. Biochem. Cell Biol. *40*, 84–97. https://doi.org/10.1016/j.biocel.2007.06.023.

24. Stutzmann, G.E., Smith, I., Caccamo, A., Oddo, S., Laferla, F.M., and Parker, I. (2006). Enhanced ryanodine receptor recruitment contributes to Ca2+ disruptions in young, adult, and aged Alzheimer's disease mice. J. Neurosci. *26*, 5180–5189. https://doi.org/10.1523/JNEUROSCI.0739-06.2006.

25. Leissring, M.A., Akbari, Y., Fanger, C.M., Cahalan, M.D., Mattson, M.P., and LaFerla, F.M. (2000). Capacitative calcium entry deficits and elevated luminal calcium content in mutant presenilin-1 knockin mice. J. Cell Biol. *149*, 793–798. https://doi.org/10.1083/jcb.149.4.793.

26. Yoo, A.S., Cheng, I., Chung, S., Grenfell, T.Z., Lee, H., Pack-Chung, E., Handler, M., Shen, J., Xia, W., Tesco, G., et al. (2000). Presenilin-mediated modulation of capacitative calcium entry. Neuron *27*, 561–572. https://doi.org/10.1016/s0896-6273(00)00066-0.

27. Green, K.N., Demuro, A., Akbari, Y., Hitt, B.D., Smith, I.F., Parker, I., and LaFerla, F.M. (2008). SERCA pump activity is physiologically regulated by presenilin and regulates amyloid beta production. J. Cell Biol. *181*, 1107–1116. https://doi.org/10.1083/jcb.200706171.

28. Chan, S.L., Mayne, M., Holden, C.P., Geiger, J.D., and Mattson, M.P. (2000). Presenilin-1 mutations increase levels of ryanodine receptors and calcium release in PC12 cells and cortical neurons. J. Biol. Chem. *275*, 18195–18200. https://doi.org/10.1074/jbc.M000040200.

29. Stutzmann, G.E., Caccamo, A., LaFerla, F.M., and Parker, I. (2004). Dysregulated IP3 signaling in cortical neurons of knock-in mice expressing an Alzheimer's-linked mutation in presenilin1 results in exaggerated Ca2+ signals and altered membrane excitability. J. Neurosci. *24*, 508–513. https://doi.org/10.1523/JNEUROSCI.4386-03.2004.

30. Tu, H., Nelson, O., Bezprozvanny, A., Wang, Z., Lee, S.F., Hao, Y.H., Serneels, L., De Strooper, B., Yu, G., and Bezprozvanny, I. (2006). Presenilins form ER Ca2+ leak channels, a function disrupted by familial Alzheimer's disease-linked mutations. Cell *126*, 981–993. https://doi.org/10.1016/j.cell.2006.06.059.

31. Baughman, J.M., Perocchi, F., Girgis, H.S., Plovanich, M., Belcher-Timme, C.A., Sancak, Y., Bao, X.R., Strittmatter, L., Goldberger, O., Bogorad, R.L., et al. (2011). Integrative genomics identifies MCU as an essential component of the mitochondrial calcium uniporter. Nature *476*, 341–345. https://doi.org/10.1038/nature10234.

32. De Stefani, D., Raffaello, A., Teardo, E., Szabò, I., and Rizzuto, R. (2011). A forty-kilodalton protein of the inner membrane is the mitochondrial calcium uniporter. Nature *476*, 336–340. https://doi.org/10.1038/nature10230.

33. Denton, R.M. (2009). Regulation of mitochondrial dehydrogenases by calcium ions. Biochim. Biophys. Acta *1787*, 1309–1316. https://doi.org/10.1016/j.bbabio.2009.01.005.

34. Duchen, M.R. (2000). Mitochondria and calcium: from cell signalling to cell death. J. Physiol. *529*, 57–68. https://doi.org/10.1111/j.1469-7793.2000.00057.x.

35. Calvo-Rodriguez, M., Hou, S.S., Snyder, A.C., Kharitonova, E.K., Russ, A.N., Das, S., Fan, Z., Muzikansky, A., Garcia-Alloza, M., Serrano-Pozo, A., et al. (2020). Increased mitochondrial calcium levels associated with neuronal death in a mouse model of Alzheimer's disease. Nat. Commun. *11*, 2146. https://doi.org/10.1038/s41467-020-16074-2.

36. Granatiero, V., Pacifici, M., Raffaello, A., De Stefani, D., and Rizzuto, R. (2019). Overexpression of mitochondrial calcium uniporter causes neuronal death. Oxid. Med. Cell. Longev. *2019*, 1681254. https://doi.org/10.1155/2019/1681254.

37. Qiu, J., Tan, Y.W., Hagenston, A.M., Martel, M.A., Kneisel, N., Skehel, P.A., Wyllie, D.J.A., Bading, H., and Hardingham, G.E. (2013). Mitochondrial calcium uniporter Mcu controls excitotoxicity and is transcriptionally repressed by neuroprotective nuclear calcium signals. Nat. Commun. *4*, 2034. https://doi.org/10.1038/ncomms3034.

38. Yao, J., Irwin, R.W., Zhao, L., Nilsen, J., Hamilton, R.T., and Brinton, R.D. (2009). Mitochondrial bioenergetic deficit precedes Alzheimer's pathology in female mouse model of Alzheimer's disease. Proc. Natl. Acad. Sci. USA *106*, 14670–14675. https://doi.org/10.1073/pnas.0903563106.

39. Chang, K.T., Niescier, R.F., and Min, K.T. (2011). Mitochondrial matrix Ca2+ as an intrinsic signal regulating mitochondrial motility in axons. Proc. Natl. Acad. Sci. USA *108*, 15456–15461. https://doi.org/10.1073/pnas.1106862108.

40. Ryan, K.C., Ashkavand, Z., and Norman, K.R. (2020). The role of mitochondrial calcium homeostasis in Alzheimer's and related diseases. Int. J. Mol. Sci. *21*, 9153. https://doi.org/10.3390/ijms21239153.

41. Britti, E., Delaspre, F., Tamarit, J., and Ros, J. (2018). Mitochondrial calcium signalling and neurodegenerative diseases. Neuronal Signal. *2*, NS20180061. https://doi.org/10.1042/NS20180061.

42. Palty, R., Silverman, W.F., Hershfinkel, M., Caporale, T., Sensi, S.L., Parnis, J., Nolte, C., Fishman, D., Shoshan-Barmatz, V., Herrmann, S., et al. (2010). NCLX is an essential component of mitochondrial Na+/Ca2+ exchange. Proc. Natl. Acad. Sci. USA *107*, 436–441. https://doi.org/10.1073/pnas.0908099107.

43. Stavsky, A., Stoler, O., Kostic, M., Katoshevsky, T., Assali, E.A., Savic, I., Amitai, Y., Prokisch, H., Leiz, S., Daumer-Haas, C., et al. (2021). Aberrant activity of mitochondrial NCLX is linked to impaired synaptic transmission and is associated with mental retardation. Commun. Biol. *4*, 666. https://doi.org/10.1038/s42003-021-02114-0.

44. Hedskog, L., Pinho, C.M., Filadi, R., Rönnbäck, A., Hertwig, L., Wiehager, B., Larssen, P., Gellhaar, S., Sandebring, A., Westerlund, M., et al. (2013). Modulation of the endoplasmic reticulum-mitochondria interface in Alzheimer's disease and related models. Proc. Natl. Acad. Sci. USA *110*, 7916–7921. https://doi.org/10.1073/pnas.1300677110.

45. Area-Gomez, E., Del Carmen Lara Castillo, M., Tambini, M.D., Guardia-Laguarta, C., de Groof, A.J.C., Madra, M., Ikenouchi, J., Umeda, M., Bird, T.D., Sturley, S.L., and Schon, E.A. (2012). Upregulated function of mitochondria-associated ER membranes in Alzheimer disease. EMBO J. *31*, 4106–4123. https://doi.org/10.1038/emboj.2012.202.

46. Sarasija, S., Laboy, J.T., Ashkavand, Z., Bonner, J., Tang, Y., and Norman, K.R. (2018). Presenilin mutations deregulate mitochondrial Ca(2+) homeostasis and metabolic activity causing neurodegeneration in Caenorhabditis elegans. Elife *7*, e33052. https://doi.org/10.7554/eLife.33052.

47. Nichols, M., Pavlov, E.V., and Robertson, G.S. (2018). Tamoxifen-induced knockdown of the mitochondrial calcium uniporter in Thy1-expressing neurons protects mice from hypoxic/ischemic brain injury. Cell Death Dis. *9*, 606. https://doi.org/10.1038/s41419-018-0607-9.

48. Luongo, T.S., Lambert, J.P., Gross, P., Nwokedi, M., Lombardi, A.A., Shanmughapriya, S., Carpenter, A.C., Kolmetzky, D., Gao, E., van Berlo, J.H., et al. (2017). The mitochondrial Na(+)/Ca(2+) exchanger is essential for Ca(2+) homeostasis and viability. Nature *545*, 93–97. https://doi.org/10.1038/nature22082.

49. Tsien, J.Z., Chen, D.F., Gerber, D., Tom, C., Mercer, E.H., Anderson, D.J., Mayford, M., Kandel, E.R., and Tonegawa, S. (1996). Subregion- and cell type-restricted gene knockout in mouse brain. Cell *87*, 1317–1326.

50. Bradley-Whitman, M.A., and Lovell, M.A. (2015). Biomarkers of lipid peroxidation in Alzheimer disease (AD): an update. Arch. Toxicol. *89*, 1035–1044. https://doi.org/10.1007/s00204-015-1517-6.

51. Butterfield, D.A., Bader Lange, M.L., and Sultana, R. (2010). Involvements of the lipid peroxidation product, HNE, in the pathogenesis and progression of Alzheimer's disease. Biochim. Biophys. Acta *1801*, 924–929. https://doi.org/10.1016/j.bbalip.2010.02.005.

52. Almeida, C.G., Tampellini, D., Takahashi, R.H., Greengard, P., Lin, M.T., Snyder, E.M., and Gouras, G.K. (2005). Beta-amyloid accumulation in APP mutant neurons reduces PSD-95 and GluR1 in synapses. Neurobiol. Dis. *20*, 187–198. https://doi.org/10.1016/j.nbd.2005.02.008.

53. Benarroch, E.E. (2018). Glutamatergic synaptic plasticity and dysfunction in Alzheimer disease: emerging mechanisms. Neurology *91*, 125–132. https://doi.org/10.1212/WNL.0000000000005807.

54. Jackson, J., Jambrina, E., Li, J., Marston, H., Menzies, F., Phillips, K., and Gilmour, G. (2019). Targeting the synapse in Alzheimer's disease. Front. Neurosci. *13*, 735. https://doi.org/10.3389/fnins.2019.00735.

55. Migaud, M., Charlesworth, P., Dempster, M., Webster, L.C., Watabe, A.M., Makhinson, M., He, Y., Ramsay, M.F., Morris, R.G., Morrison, J.H., et al. (1998). Enhanced long-term potentiation and impaired learning in mice with mutant postsynaptic density-95 protein. Nature *396*, 433–439. https://doi.org/10.1038/24790.

56. Zhang, P., and Lisman, J.E. (2012). Activity-dependent regulation of synaptic strength by PSD-95 in CA1 neurons. J. Neurophysiol. *107*, 1058–1066. https://doi.org/10.1152/jn.00526.2011.

57. Cameron, P.L., Südhof, T.C., Jahn, R., and De Camilli, P. (1991). Colocalization of synaptophysin with transferrin receptors: implications for synaptic vesicle biogenesis. J. Cell Biol. *115*, 151–164. https://doi.org/10.1083/jcb.115.1.151.

58. Kwon, S.E., and Chapman, E.R. (2011). Synaptophysin regulates the kinetics of synaptic vesicle endocytosis in central neurons. Neuron *70*, 847–854. https://doi.org/10.1016/j.neuron.2011.04.001.

59. Habib, N., McCabe, C., Medina, S., Varshavsky, M., Kitsberg, D., Dvir-Szternfeld, R., Green, G., Dionne, D., Nguyen, L., Marshall, J.L., et al. (2020). Disease-associated astrocytes in Alzheimer's disease and aging. Nat. Neurosci. *23*, 701–706. https://doi.org/10.1038/s41593-020-0624-8.

60. Park, J.S., Kam, T.I., Lee, S., Park, H., Oh, Y., Kwon, S.H., Song, J.J., Kim, D., Kim, H., Jhaldiyal, A., et al. (2021). Blocking microglial activation of reactive astrocytes is neuroprotective in models of

Alzheimer's disease. Acta Neuropathol. Commun. *9*, 78. https://doi.org/10.1186/s40478-021-01180-z.

61. Caruso, D., Barron, A.M., Brown, M.A., Abbiati, F., Carrero, P., Pike, C.J., Garcia-Segura, L.M., and Melcangi, R.C. (2013). Age-related changes in neuroactive steroid levels in 3xTg-AD mice. Neurobiol. Aging *34*, 1080–1089. https://doi.org/10.1016/j.neurobiolaging.2012.10.007.

62. Du, H., Guo, L., Fang, F., Chen, D., Sosunov, A.A., McKhann, G.M., Yan, Y., Wang, C., Zhang, H., Molkentin, J.D., et al. (2008). Cyclophilin D deficiency attenuates mitochondrial and neuronal perturbation and ameliorates learning and memory in Alzheimer's disease. Nat. Med. *14*, 1097–1105. https://doi.org/10.1038/nm.1868.

63. Szalai, G., Krishnamurthy, R., and Hajnóczky, G. (1999). Apoptosis driven by IP(3)-linked mitochondrial calcium signals. EMBO J. *18*, 6349–6361. https://doi.org/10.1093/emboj/18.22.6349.

64. Nakagawa, T., Zhu, H., Morishima, N., Li, E., Xu, J., Yankner, B.A., and Yuan, J. (2000). Caspase-12 mediates endoplasmic-reticulum-specific apoptosis and cytotoxicity by amyloid-beta. Nature *403*, 98–103. https://doi.org/10.1038/47513.

65. Luongo, T.S., Lambert, J.P., Yuan, A., Zhang, X., Gross, P., Song, J., Shanmughapriya, S., Gao, E., Jain, M., Houser, S.R., et al. (2015). The mitochondrial calcium uniporter matches energetic supply with cardiac workload during stress and modulates permeability transition. Cell Rep. *12*, 23–34. https://doi.org/10.1016/j.celrep.2015.06.017.

66. Schinder, A.F., Olson, E.C., Spitzer, N.C., and Montal, M. (1996). Mitochondrial dysfunction is a primary event in glutamate neurotoxicity. J. Neurosci. *16*, 6125–6133.

67. Okonkwo, D.O., Büki, A., Siman, R., and Povlishock, J.T. (1999). Cyclosporin A limits calcium-induced axonal damage following traumatic brain injury. Neuroreport *10*, 353–358. https://doi.org/10.1097/00001756-199902050-00026.

68. Uchino, H., Elmér, E., Uchino, K., Lindvall, O., and Siesjö, B.K. (1995). Cyclosporin A dramatically ameliorates CA1 hippocampal damage following transient forebrain ischaemia in the rat. Acta Physiol. Scand. *155*, 469–471. https://doi.org/10.1111/j.1748-1716.1995.tb09999.x.

69. Matsuura, K., Kabuto, H., Makino, H., and Ogawa, N. (1996). Cyclosporin A attenuates degeneration of dopaminergic neurons induced by 6-hydroxydopamine in the mouse brain. Brain Res. *733*, 101–104. https://doi.org/10.1016/0006-8993(96)00686-5.

70. Caspersen, C., Wang, N., Yao, J., Sosunov, A., Chen, X., Lustbader, J.W., Xu, H.W., Stern, D., McKhann, G., and Yan, S.D. (2005). Mitochondrial Abeta: a potential focal point for neuronal metabolic dysfunction in Alzheimer's disease. FASEB J *19*, 2040–2041. https://doi.org/10.1096/fj.05-3735fje.

71. Raffaello, A., De Stefani, D., Sabbadin, D., Teardo, E., Merli, G., Picard, A., Checchetto, V., Moro, S., Szabò, I., and Rizzuto, R. (2013). The mitochondrial calcium uniporter is a multimer that can include a dominant-negative pore-forming subunit. EMBO J. *32*, 2362–2376. https://doi.org/10.1038/emboj.2013.157.

72. Mallilankaraman, K., Doonan, P., Cárdenas, C., Chandramoorthy, H.C., Müller, M., Miller, R., Hoffman, N.E., Gandhirajan, R.K., Molgó, J., Birnbaum, M.J., et al. (2012). MICU1 is an essential gatekeeper for MCU-mediated mitochondrial Ca(2+) uptake that regulates cell survival. Cell *151*, 630–644. https://doi.org/10.1016/j.cell.2012.10.011.

73. Patron, M., Checchetto, V., Raffaello, A., Teardo, E., Vecellio Reane, D., Mantoan, M., Granatiero, V., Szabò, I., De Stefani, D., and Rizzuto, R. (2014). MICU1 and MICU2 finely tune the mitochondrial Ca2+ uniporter by exerting opposite effects on MCU activity. Mol. Cell *53*, 726–737. https://doi.org/10.1016/j.molcel.2014.01.013.

74. Debattisti, V., Horn, A., Singh, R., Seifert, E.L., Hogarth, M.W., Mazala, D.A., Huang, K.T., Horvath, R., Jaiswal, J.K., and Hajnóczky, G. (2019). Dysregulation of mitochondrial Ca(2+) uptake and sarcolemma repair underlie muscle weakness and wasting in patients and mice lacking MICU1. Cell Rep. *29*, 1274–1286.e6. https://doi.org/10.1016/j.celrep.2019.09.063.

75. Lewis-Smith, D., Kamer, K.J., Griffin, H., Childs, A.M., Pysden, K., Titov, D., Duff, J., Pyle, A., Taylor, R.W., Yu-Wai-Man, P., et al. (2016). Homozygous deletion in MICU1 presenting with fatigue and lethargy in childhood. Neurol. Genet. *2*, e59. https://doi.org/10.1212/NXG.0000000000000059.

76. Logan, C.V., Szabadkai, G., Sharpe, J.A., Parry, D.A., Torelli, S., Childs, A.M., Kriek, M., Phadke, R., Johnson, C.A., Roberts, N.Y., et al. (2014). Loss-of-function mutations in MICU1 cause a brain and muscle disorder linked to primary alterations in mitochondrial calcium signaling. Nat. Genet. *46*, 188–193. https://doi.org/10.1038/ng.2851.

77. Wilton, K.M., Morales-Rosado, J.A., Selcen, D., Muthusamy, K., Ewing, S., Agre, K., Nickels, K., Klee, E.W., Ho, M.L., and Morava, E. (2020). Developmental brain abnormalities and acute encephalopathy in a patient with myopathy with extrapyramidal signs secondary to pathogenic variants in MICU1. JIMD Rep. *53*, 22–28. https://doi.org/10.1002/jmd2.12114.

78. Bitarafan, F., Khodaeian, M., Amjadi Sardehaei, E., Darvishi, F.Z., Almadani, N., Nilipour, Y., and Garshasbi, M. (2021). Identification of a novel MICU1 nonsense variant causes myopathy with extrapyramidal signs in an Iranian consanguineous family. Mol. Cell. Pediatr. *8*, 6. https://doi.org/10.1186/s40348-021-00116-w.

79. Kohlschmidt, N., Elbracht, M., Czech, A., Häusler, M., Phan, V., Töpf, A., Huang, K.T., Bartok, A., Eggermann, K., Zippel, S., et al. (2021). Molecular pathophysiology of human MICU1 deficiency. Neuropathol. Appl. Neurobiol. *47*, 840–855. https://doi.org/10.1111/nan.12694.

80. Antony, A.N., Paillard, M., Moffat, C., Juskeviciute, E., Correnti, J., Bolon, B., Rubin, E., Csordás, G., Seifert, E.L., Hoek, J.B., and Hajnóczky, G. (2016). MICU1 regulation of mitochondrial Ca(2+) uptake dictates survival and tissue regeneration. Nat. Commun. *7*, 10955. https://doi.org/10.1038/ncomms10955.

81. Liu, J.C., Liu, J., Holmström, K.M., Menazza, S., Parks, R.J., Fergusson, M.M., Yu, Z.X., Springer, D.A., Halsey, C., Liu, C., et al. (2016). MICU1 serves as a molecular gatekeeper to prevent in vivo mitochondrial calcium overload. Cell Rep. *16*, 1561–1573. https://doi.org/10.1016/j.celrep.2016.07.011.

82. Jadiya, P., Kolmetzky, D.W., Tomar, D., Thomas, M., Khaledi, S., Garbincius, J.F., Hildebrand, A.N., and Elrod, J.W. (2021). Genetic Ablation of Neuronal Mitochondrial Calcium Uptake Halts Alzheimer's Disease Progression (SSRN). https://doi.org/10.2139/ssrn.3872940.

83. Nichols, B.J., and Denton, R.M. (1995). Towards the molecular basis for the regulation of mitochondrial dehydrogenases by calcium ions. Mol. Cell. Biochem. *149–150*, 203–212. https://doi.org/10.1007/BF01076578.

84. Panel, M., Ghaleh, B., and Morin, D. (2018). Mitochondria and aging: a role for the mitochondrial transition pore? Aging Cell *17*, e12793. https://doi.org/10.1111/acel.12793.

85. Duan, Y., Gross, R.A., and Sheu, S.S. (2007). Ca2+-dependent generation of mitochondrial reactive oxygen species serves as a signal for poly(ADP-ribose) polymerase-1 activation during glutamate excitotoxicity. J. Physiol. *585*, 741–758. https://doi.org/10.1113/jphysiol.2007.145409.

86. Starkov, A.A., Chinopoulos, C., and Fiskum, G. (2004). Mitochondrial calcium and oxidative stress as mediators of ischemic brain injury. Cell Calcium *36*, 257–264. https://doi.org/10.1016/j.ceca.2004.02.012.

87. Tong, Y., Zhou, W., Fung, V., Christensen, M.A., Qing, H., Sun, X., and Song, W. (2005). Oxidative stress potentiates BACE1 gene expression and Abeta generation. J. Neural. Transm. *112*, 455–469. https://doi.org/10.1007/s00702-004-0255-3.

88. Tönnies, E., and Trushina, E. (2017). Oxidative stress, synaptic dysfunction, and Alzheimer's disease. J. Alzheimers Dis. *57*, 1105–1121. https://doi.org/10.3233/JAD-161088.

89. Gandhi, S., Wood-Kaczmar, A., Yao, Z., Plun-Favreau, H., Deas, E., Klupsch, K., Downward, J., Latchman, D.S., Tabrizi, S.J., Wood, N.W., et al. (2009). PINK1-associated Parkinson's disease is caused by neuronal vulnerability to calcium-induced cell death.

Mol. Cell *33*, 627–638. https://doi.org/10.1016/j.molcel.2009.02.013.

90. Nakamura, T., and Lipton, S.A. (2017). 'SNO'-Storms compromise protein activity and mitochondrial metabolism in neurodegenerative disorders. Trends Endocrinol. Metab. *28*, 879–892. https://doi.org/10.1016/j.tem.2017.10.004.

91. Chouchani, E.T., Hurd, T.R., Nadtochiy, S.M., Brookes, P.S., Fearnley, I.M., Lilley, K.S., Smith, R.A.J., and Murphy, M.P. (2010). Identification of S-nitrosated mitochondrial proteins by S-nitrosothiol difference in gel electrophoresis (SNO-DIGE): implications for the regulation of mitochondrial function by reversible S-nitrosation. Biochem. J. *430*, 49–59. https://doi.org/10.1042/BJ20100633.

92. Gupta, K.J., Shah, J.K., Brotman, Y., Jahnke, K., Willmitzer, L., Kaiser, W.M., Bauwe, H., and Igamberdiev, A.U. (2012). Inhibition of aconitase by nitric oxide leads to induction of the alternative oxidase and to a shift of metabolism towards biosynthesis of amino acids. J. Exp. Bot. *63*, 1773–1784. https://doi.org/10.1093/jxb/ers053.

93. Sun, J., Morgan, M., Shen, R.F., Steenbergen, C., and Murphy, E. (2007). Preconditioning results in S-nitrosylation of proteins involved in regulation of mitochondrial energetics and calcium transport. Circ. Res. *101*, 1155–1163. https://doi.org/10.1161/CIRCRESAHA.107.155879.

94. Zhang, J., Jin, B., Li, L., Block, E.R., and Patel, J.M. (2005). Nitric oxide-induced persistent inhibition and nitrosylation of active site cysteine residues of mitochondrial cytochrome-c oxidase in lung endothelial cells. Am. J. Physiol. Cell Physiol. *288*, C840–C849. https://doi.org/10.1152/ajpcell.00325.2004.

95. Stokin, G.B., Lillo, C., Falzone, T.L., Brusch, R.G., Rockenstein, E., Mount, S.L., Raman, R., Davies, P., Masliah, E., Williams, D.S., and Goldstein, L.S.B. (2005). Axonopathy and transport deficits early in the pathogenesis of Alzheimer's disease. Science *307*, 1282–1288. https://doi.org/10.1126/science.1105681.

96. Calkins, M.J., Manczak, M., Mao, P., Shirendeb, U., and Reddy, P.H. (2011). Impaired mitochondrial biogenesis, defective axonal transport of mitochondria, abnormal mitochondrial dynamics and synaptic degeneration in a mouse model of Alzheimer's disease. Hum. Mol. Genet. *20*, 4515–4529. https://doi.org/10.1093/hmg/ddr381.

97. Cai, Q., and Tammineni, P. (2016). Alterations in mitochondrial quality control in Alzheimer's disease. Front. Cell. Neurosci. *10*, 24. https://doi.org/10.3389/fncel.2016.00024.

98. Boscia, F., Pannaccione, A., Ciccone, R., Casamassa, A., Franco, C., Piccialli, I., de Rosa, V., Vinciguerra, A., Di Renzo, G., and Annunziato, L. (2017). The expression and activity of KV3.4 channel subunits are precociously upregulated in astrocytes exposed to Abeta oligomers and in astrocytes of Alzheimer's disease Tg2576 mice. Neurobiol. Aging *54*, 187–198. https://doi.org/10.1016/j.neurobiolaging.2017.03.008.

99. Pannaccione, A., Piccialli, I., Secondo, A., Ciccone, R., Molinaro, P., Boscia, F., and Annunziato, L. (2020). The Na(+)/Ca(2+) exchanger in Alzheimer's disease. Cell Calcium *87*, 102190. https://doi.org/10.1016/j.ceca.2020.102190.

100. Kostic, M., Ludtmann, M.H.R., Bading, H., Hershfinkel, M., Steer, E., Chu, C.T., Abramov, A.Y., and Sekler, I. (2015). PKA phosphorylation of NCLX reverses mitochondrial calcium overload and depolarization, promoting survival of PINK1-deficient dopaminergic neurons. Cell Rep. *13*, 376–386. https://doi.org/10.1016/j.celrep.2015.08.079.

101. Tomar, D., Dong, Z., Shanmughapriya, S., Koch, D.A., Thomas, T., Hoffman, N.E., Timbalia, S.A., Goldman, S.J., Breves, S.L., Corbally, D.P., et al. (2016). MCUR1 is a scaffold factor for the MCU complex function and promotes mitochondrial bioenergetics. Cell Rep. *15*, 1673–1685. https://doi.org/10.1016/j.celrep.2016.04.050.

102. Zhang, L., Li, J., and Lin, A. (2021). Assessment of neurodegeneration and neuronal loss in aged 5XFAD mice. STAR Protoc. *2*, 100915. https://doi.org/10.1016/j.xpro.2021.100915.

STAR★METHODS

KEY RESOURCES TABLE

REAGENT or RESOURCE	SOURCE	IDENTIFIER
Experimental models: Organisms/strains		
NCLX$^{fl/fl}$ mice	Luongo et al.,[48]	N/A
B6.Cg-Tg(Camk2a-cre)T291-Stl/J	The Jackson Laboratory, USA	Stock # 005359
NCLX$^{fl/fl}$ x Camk2a-Cre	This Study	N/A
Antibodies		
MCU (1:1000)	Sigma	Cat # HPA016480
MCUb (1:1000)	Abgent	Cat # AP12355b
MICU1 (1:500)	Tomar et al.,[101]	Custom generation by Yenzyme
MICU2 (1:500)	Abcam	Cat # ab101465
MICU3 (1:500)	Sigma Aldrich	Cat # HPA024771
EMRE (1:1000)	Santa Cruz Biotechnology Inc.	Cat # sc-86337
NCLX (1:500)	Santa Cruz Biotechnology Inc.	Cat # sc-161921
VDAC (1:2500)	Abcam	Cat # ab15895
OxPhos Cocktail	Abcam	Cat # MS604
Total APP (22C11, 1:1500)	Chemicon International	Cat # MAB348
BACE1 (1:500)	Sigma	Cat # MAB5308
ADAM10 (1:500)	Chemicon International	Cat # AB19026
PS1 (1:500)	Sigma	Cat #S182
Nicastrin (1:200)	Cell Signaling	Cat # 5665
APH-1 (1:200)	Millipore	Cat # AB9214
HT7 (1:200)	Thermo Fisher Scientific	Cat # MN1000
AT180 (1:200)	Thermo Fisher Scientific	Cat # MN1040
AT8 (1:200)	Thermo Fisher Scientific	Cat # MN1020
AT270 (1:200)	Thermo Fisher Scientific	Cat # MN1050
PHF13 (1:200)	Cell Signaling	Cat # 9632
4-HNE	Abcam	Cat # ab48506
SYP (1:500)	Santa Cruz Biotechnology	Cat # sc-55507
IBA-1 (1: 250)	Proteintech	Cat # 10904-1-AP
PSD-95 (1:250)	Invitrogen	Cat # MA1-045
GFAP	Proteintech	Cat # 60190-1-Ig
Beta-Tubulin (1: 1000)	Abcam	Cat # ab6046
Anti-Mouse (1:10000)	Licor	Cat # 925–68070
Anti-Goat (1:10000)	Licor	Cat # 926-32214
Anti-Rabbit (1:10,000)	Licor	Cat # 926–32211
Oligonucleotides		
Rps13-F	GCACCTTGAGAGGAACAGAA	N/A
Rps13-R	GAGCACCCGCTTAGTCTTATAG	N/A
Nclx-F	GCCATCTCCACTAACCTCAAA	N/A
Nclx-R	GGGTCTGAGAAAGCCACTAAA	N/A

(*Continued on next page*)

Continued

REAGENT or RESOURCE	SOURCE	IDENTIFIER
Recombinant DNA		
gRNA #1	GGGCCTCTACGTGTTCTACGGTTTTAGAG CTAGAAATAGCAAGTTAAAATAAGGCTAG TCCGTTATCAACTTGAAAAAGTGGCACCG AGTCGGTGC	N/A
gRNA #2	CTCACCTGGTGTCTCCGATAGTTTTAGAG CTAGAAATAGCAAGTTAAAATAAGGCTAG TCCGTTATCAACTTGAAAAAGTGGCACCG AGTCGGTGC	N/A
Chemicals, peptides, and recombinant proteins		
Paraformaldehyde	Sigma	Cat #P6148
Vector Elite ABC HRP Kit	Vector Laboratory	Cat # PK-6100
DAB Substrate Kit	BD Biosciences	Cat # 550880
RIPA buffer	EMD-Millipore	Cat # 20-188
SIGMAFAST™ Protease Inhibitor Cocktail	Sigma-Aldrich	Cat #S8830
Phosphatase inhibitor	Sigma-Aldrich	Cat # 04906837001
Formic acid	Sigma	Cat # 33015
Human Aβ (1-40) ELISA Kit	Wako Chemicals USA	Cat # 298-64601
Human Aβ (1-42) ELISA Kit	Wako Chemicals USA	Cat # 298-62401
Protein Assay Dye Reagent	Bio-Rad	Cat # 22660
PVDF Immobilon-FL membrane	EMD Millipore	Cat # IPFL00010
Blocking buffer	Rockland	Cat # MB-070
Dihydroethidium (DHE)	Thermo Fisher Scientific	Cat #D11347
KCl	Sigma-Aldrich	Cat #P9333
Cresyl Violet	Sigma-Aldrich	Cat# C5042
Glacial acetic acid	Sigma-Aldrich	Cat# A6283
KH_2PO_4	Sigma-Aldrich	Cat #P5655
$MgCl_2$	Sigma-Aldrich	Cat # 449172
NaCl	Sigma-Aldrich	Cat # 746398
DAPI	Thermo Fisher Scientific	Cat #P36981
Software and algorithms		
Fiji ImageJ software	Fiji ImageJ	https://imagej.net/software/fiji/
Zen 2010	Carl Zeiss	https://www.zeiss.com/microscopy/en/products/software/zeiss-zen.html
GraphPad Prism 9	GraphPad Software	https://www.graphpad.com/scientific-software/prism/
ImageJ Pro plus software	Meyer Instruments	https://www.meyerinst.com/mediacybernetics/image-pro-plus/
PACKWIN software	Harvard Apparatus	https://www.harvardapparatus.com/packwin-software-panlab.html

RESOURCE AVAILABILITY

Lead contact

Further information and requests for resources should be directed to and will be fulfilled by the corresponding author, John W. Elrod (elrod@temple.edu).

Materials availability

All reagents and mice generated in this study are available from the lead contact, J.W.E. (elrod@temple.edu).

Data and code availability

- The data reported in this paper will be shared by the lead contact upon request.
- This paper does not report original code.
- Any additional information required to reanalyze the data reported in this paper is available from the lead contact upon request.

EXPERIMENTAL MODEL AND SUBJECTDETAILS

Neuronal-specific NCLX knockout (*NCLX*$^{fl/fl}$ x Camk2a-Cre) mouse

NCLX floxed mice were generated by our lab by acquiring targeted ES cells made by recombinant insertion of a construct containing loxP sites flanking exons 5 - 7 of the *NCLX, Slc8b1* gene (ch12: 113298759-113359493).[48] *NCLX*$^{fl/fl}$ mice were crossed with Camk2a-Cre mice (expression of Cre recombinase directed by calcium/calmodulin-dependent protein kinase II alpha promoter, primarily in the prefrontal cortex and CA1 layer of the hippocampus)[49] to generate neuron-specific *NCLX* knockouts (NCLX-nKO; *NCLX*$^{fl/fl}$ x Camk2a-Cre). Animal studies were approved by Temple University's IACUC and followed AAALAC guidelines. We used both male and female mice of different ages (2, 6, 9, 15, and 16m, depending on the assay) for this study.

METHOD DETAILS

Immunohistochemistry

Mouse brains from NCLX-nKO (*NCLX*$^{fl/fl}$ x Camk2a-Cre) and control (Camk2a-Cre) mice were prepared for immunohistochemistry.[18] In brief, brains were fixed in 4% paraformaldehyde overnight, embedded in paraffin, and sectioned. 6-μm thick coronal sections were then deparaffinized, hydrated, and blocked in 2% fetal bovine serum. The sections were incubated with primary antibody overnight at 4°C. The primary antibodies and dilutions were as follows: HT7 dilution 1:150 (Thermo Fisher Scientific, Catalog # MN1000), phospho-tau (pThr231) monoclonal AT180 dilution 1:50 (Thermo Fisher Scientific, Catalog # MN1040) and anti-4 hydroxynonenal antibody (4-HNE) dilution 1:20 (Abcam, Catalog # ab48506). The sections were then incubated with secondary antibodies and developed using the Vector Elite ABC (Avidin-Biotin Complex) system (Vector Laboratories Inc., Burlingame, CA).

Biochemical and western blot analysis

Brains harvested from NCLX-nKO (*NCLX*$^{fl/fl}$ x Camk2a-Cre) and control mice (Camk2a-Cre) were homogenized in 1x RIPA lysis buffer with SIGMAFAST™ Protease Inhibitor Cocktail and phosphatase inhibitor. Lysates were centrifuged and the supernatant (soluble fraction) collected. The pellet was further lysed in 70% formic acid, sonicated, and centrifuged to collect the insoluble fraction. The resulting supernatant (insoluble fraction) was neutralized with 6 N sodium hydroxide. The lysates were centrifuged for 45 min at 4°C, and the supernatant was used as the soluble fraction. To get the insoluble fraction, the pellet was further lysed in 70% formic acid, sonicated, and centrifuged for 45 min at 4°C. The resulting supernatant (representing the insoluble fraction) was neutralized with 6 N sodium hydroxide. The soluble and insoluble fractions were assayed for $A\beta_{1-40}$ and $A\beta_{1-42}$ levels using sandwich ELISA (Wako Chemicals USA, Inc.) according to manufacturer instructions. Data were presented as a percentage change of $A\beta_{1-40}$ and $A\beta_{1-42}$ relative to controls.

For Western blot analysis, the protein concentration in the soluble fraction was determined by a Bio-Rad Protein Assay Dye Reagent. Equal amounts of protein (25-30 μg) were resolved using SDS-polyacrylamide gel electrophoresis (SDS-PAGE). After transferring protein from the gel to the PVDF Immobilon-FL membrane, the membrane was incubated in blocking buffer for 1 hrat room temperature, followed by incubation with primary antibody at 4°C overnight and then with specific Licor IR secondary antibody for 1 hr at room temperature. Licor Odyssey system was used to scan all blots and all full-length western blots are available in Figure S3.

Memory tests

Mice from NCLX-nKO (*NCLX*$^{fl/fl}$ x Camk2a-Cre) and controls (Camk2a-Cre) at 6-, 9-, 12-, and 15-months of age were assessed in the following cognition function tests.

Y-maze of spontaneous alternation

The Y-maze was used to assess spontaneous alternation, a measure of spatial working memory in mice, by allowing the test animals to explore all three arms of the Y-shaped maze (San Diego Instruments, 32 cm (long) 610 cm (wide) with 26-cm walls) for 5 min. The mice were tested for the total number of arms entries and for the three-consecutive sequence of entries (i.e., 1, 2, 3, or 2, 3, 1, or 3,1,2) to calculate percentage alternations using the formula ''total alternation number/(total number of entries-2) × 100''.[18]

Contextual and cued fear conditioning

This test took place in a fear-conditioning apparatus (StartFear, Panlab Harvard Apparatus, 25 cm height × 30 cm width × 25 cm depth) on two consecutive days as described.[18] During the training phase (Day 1), animals were placed in the chamber, and baseline freezing was recorded during a 6-min time interval with three cycles of 30s of sound and 10 s of electric shock (1.5mA). During the memory test phase (Day 2), mice were assessed for two trials, contextual and cued memory. For the contextual test, mice spent 5 min in the same chamber used during training, but without tones or electric shocks, and freezing behavior was recorded. For the cued test, two hours following the contextual test mice were placed in the same chamber with a modified environment such as different walls, smells, lighting, flooring, sound and freezing behavior was recorded for 6 min. Differences in freezing time between groups were analyzed via PACKWIN (Panlab, Harvard Apparatus, USA).

Rotarod test

To assess motor coordination, mice from controls and NCLX-nKO groups were tested using the rotarod test. During the training phase (Day 1-3), mice were placed on the rotarod apparatus initially at speed 0 rpm (30 s) and then at a constant speed 4 rpm (60 s), up to 6 trials per day with a 30 min rest period between each trial. During the test phase (Day 4), the rotarod started at speed 0 and accelerated to 90 rpm over a period of 90 s. The latency to falling off the rod was recorded on each day.

Assessment of lipid peroxidation

To measure redox stress, we performed 4-hydroxy-2-nonenal (4-HNE) staining. Mouse brains were prepared for immunohistochemistry as described above. The deparaffinized brain tissue sections of 16-month-old NCLX-nKO and controls were subjected to endogenous peroxidase quenched with 5% H_2O_2 in methanol for 30 minutes, followed by washing thrice in TBS-X (TBS and 0.3% Triton X-100) buffer for 5 minutes. Sections were treated with blocking buffer (2 % fetal bovine serum in TBS-X for overnight at 4°C) and incubated with primary 4-HNE antibody (dilution 1:20) overnight at 4°C in a humidified chamber. The next day, after washing with TBS-X thrice for 5 minutes, tissues were incubated with a biotinylated anti-mouse IgG for 1 hour in a humidified chamber and subsequently developed using an avidin-biotin-peroxidase complex, and the peroxidase activity was visualized using a stable DAB (diaminobenzidine) solution. Immunoreactivity was visualized using a light microscope and images were quantified using the Image-Pro Plus software.

Nissl staining

Nissl staining to examine neuronal density was performed in NCLX-nKO and control brain sections using 0.5% Cresyl violet acetate solution that stains Nissl substance in the cytoplasm of neurons.[102] Imaging was performed using a whole slide imager Olympus VS-110 at the 40x resolution. Neuronal density was calculated in a given area of cells/mm^2 using Fiji Image J software and presented as percentage change vs. Camk2a-Cre controls.

Cell culture and generation of NCLX knockout cells

Mouse neuroblastoma Neuro-2a cells (N2a) were grown in Dulbecco's modified Eagle's medium supplemented with 10% fetal bovine serum (peak serum) and 1% penicillin/streptomycin (gibco) at 37 °C in the presence of 5% CO_2. For the generation of NCLX knockout (NCLX-/-) cells, N2a cells were transfected with a mammalian expression plasmid (VectorBuilder) encoding 2 gRNA's under the direction of the U6 promoter, human codon-optimized cas9 (also known as SpCas9) under the direction of the CBh promoter

(CMV early enhancer fused to modified chicken β-actin promoter), and hygromycin resistance via electroporation. 48 hours following electroporation, hygromycin was added to culture media (200 μg/ml). Clonal populations were grown up from the bulk transfected population and screened via qPCR.

qPCR mRNA analysis

RNA was extracted using the Qiagen RNeasy kit. cDNA was generated from 1ug of RNA using the High-Capacity cDNA Reverse Transcription Kit (Applied Biosystems). qPCR was conducted according to manufacturer instructions (PowerUp SYBR Green Master Mix, Applied Biosystems). All reactions were run in triplicate and RPS13 was used as a housekeeping gene. For validation of NCLX knock-out cell lines, Exon-spanning qPCR primers were designed to amplify the junction between exons 8 and 9. $2^{\wedge\Delta\Delta Ct}$ was calculated to determine NCLX mRNA expression relative to WT control.

Quantification of $_{m}Ca^{2+}$ content and retention capacity

For evaluation of $_{m}Ca^{2+}$ retention capacity and content, cells were cultured and transferred to an intracellular-like medium (120mM KCl, 10mM NaCl, 1mM KH2PO4, 20mM HEPES-Tris, pH 7.2) containing digitonin (80-μg/ml) to permeabilize the plasma membrane, thapsigargin (3 μM) to inhibit SERCA so that the movement of Ca^{2+} was only influenced by mitochondria, protease inhibitors (Sigma EGTA-Free cocktail), and succinate (5 mM). All solutions used were cleared of trace Ca^{2+} with Chelex 100 (Sigma). For evaluation of $_{m}Ca^{2+}$ content: 2 million digitonin-permeabilized neuronal cells were loaded with the ratiometric calcium reporter Fura-2 (Invitrogen, 1μM) to monitor extramitochondrial Ca^{2+} and Ru360 (10 μM) and CGP-37157 (10 μM) to inhibit $_{m}Ca^{2+}$ uptake and efflux, respectively. At 250 s. Carbonyl cyanide-p-trifluoromethoxyphenylhydrazone (FCCP) was added to rapidly collapse mitochondrial membrane potential, causing Ca^{2+} to evacuate the matrix. Fluorescent signals were monitored in a spectrofluorometer (Delta RAM, Photon Technology Int.) at 380/510 excitation/emmision For evaluation of $_{m}Ca^{2+}$ retention capacity cells were transferred to an intracellular-like medium containing thapsigargin and digitonin and loaded with the ratiometric Ca^{2+} reporter FuraFF (Cayman Chemical Company, 1 μM) to monitor extramitochondrial Ca^{2+} and JC-1 (Enzo Life Sciences, 4.8 μM) to monitor mitochondrial membrane potential. At 400s a repetitive series of 10μM Ca^{2+} boluses were added at the indicated time points until spontaneous Ca release, at which point 1 μM FCCP was added.

Membrane rupture assay

The propensity for neuronal death was evaluated using membrane rupture upon exposure to apoptotic agonists. Membrane rupture was quantified using sytox green (life technologies), a cell impermeant dye that enters the cell upon membrane rupture and intercalates DNA causing > 500-fold increase in fluorescent emission. Equal numbers of cells were plated in each well of a 96-well plate. After 24 hours, culture media was replaced with calcium ionophore ionomycin or thapsigargin at the indicated concentrations. After 24 hours, cells were loaded with 10 μM Sytox green for 30 minat 37 °C and measured the fluorescence at 504/523 ex/em using a Tecan Infinite M1000 Pro plate reader. Data are normalized to vehicle control to avoid any differences in cell numbers between the groups.

Detection of protein aggregation

Detection of protein aggregation was done using Proteostat protein aggregation kit (Enzo Life Sciences) according to manufacturer instructions. Proteostat recognizes the β-sheet structure of aggregated and misfolded proteins. In brief, cells were grown on 35 mm glass bottom cell culture dishes, fixed with 4% paraformaldehyde, permeabilized using a buffer containing 0.5% Triton X-100, 3mM EDTA, pH 8.0, and stained using proteostat aggresome detection dye and Hoechst 33342 nuclear counterstain for 30 min at RT. Stained cells were imaged on a ZEISS LSM 900 microscope using a 40x objective with appropriate laser settings for aggresome and nuclear signals. Proteostat staining intensity per cell was quantified using CellProfiler.

QUANTIFICATION AND STATISTICAL ANALYSIS

For statistical analysis, Graph Pad Prism 9.0 software was used. All experiments were performed thrice, and results were presented as mean ± SEM. Where appropriate, column analyses were performed using an unpaired, two-tailed *t*-test or two-way ANOVA multiple comparisons testing for an age effect with Dunnett's post-hoc test for comparison to age 6 months and comparison of genotype across all ages using Bonferroni's multiple comparisons tests. Results were significant if p values < 0.05 (95% confidence interval).